June 1986 LRP 286/86

STABILITY OF SINGLE-MODE OPTICALLY PUMPED LASERS

M.A. Dupertruis, M.R. Siegrist and R.R.E. Salomaa

submitted for publication to IEEE Journal of Quantum Electronics

STABILITY OF SINGLE-MODE OPTICALLY PUMPED LASERS

M.A. Dupertuis * and M.R. Siegrist

Centre de Recherches en Physique des Plasmas,
Association EURATOM - Confédération Suisse,
Ecole Polytechnique Fédérale de Lausanne,
21, Av. des Bains, CH-1007 Lausanne, Switzerland

R.R.E. Salomaa, Department of Technical Physics,
Helsinki University of Technology, SF-02150 Espoo, Finland

* Presently at : Research Institute for Theoretical Physics,
University of Helsinki,
Siltavuorenpenger 20C, SF-00170 Helsinki, Finland

ABSTRACT

We study mode competition in optically pumped lasers with one active laser line. The stability of single mode operation under one mode pumping (both fields arbitrarily intense) is determined by calculating the saturated laser gain using either a mono- or bichromatic probe. The probe spectra differ dramatically from the single mode, intense field gain curves occasionally exploited in this context in earlier works. Some features in the spectra are interpreted with the dressed atom picture. The mathematically simpler single probe gain is shown to be a good approximation for large mode spacings. When the strong field induced Rabi flipping is comparable to the mode spacing, however, a bichromatic probe containing two frequencies which are symmetric with respect to the intense mode is usually needed. Typical mono- and bichromatic probe spectra are discussed and parameter regions are explored which give stable single-mode operation. The results are also relevant in general laser instability studies : some aspects due to the strong field induced coherences will be pointed out.

I. INTRODUCTION

The coarsest level of oscillation competition in lasers pumped by off-resonant coherent light occurs in line selection between line center and stimulated Raman emission. On a finer scale several cavity eigenmodes may appear within the gain bands of the two above mentioned lines. This is a typical situation for instance in most pulsed far infrared (FIR) lasers. Usually these types of lasers operate preferentially on the Raman line which allows their tunability by pump tuning. In several practical applications (e.g. plasma diagnostics, high resolution spectroscopy) it is desirable to have single mode operation in addition to tunability.

One means to explore the parameter regions giving rise to single mode operation is to use a weak tunable probe and study its stability in the presence of the presumed arbitrarily intense oscillating mode. If the probe experiences damping at all its allowed parameter values, single mode operation is proven to be stable. Otherwise cavity modes located in the positive probe gain regions are able to grow from noise.

During the initial growth transient in an unstable situation the reaction of the unstable modes back onto the established main mode may be ignored. Hence the study of linearized probe gain spectra provides valuable insight for instance into the problematics of the low level line width of FIR lasers [1]. Dispersion must also be considered in this context in addition to gain. Instabilities in homogeneously broadened lasers are another possible field of application which is of great current interest because of its relation to the nonlinear dynamical effects in lasers, ranging from regular spiking to the onset of full chaos (see e.g. [2,3]).

Single mode characteristics of FIR and other types of optically pumped lasers have extensively been studied in the literature (see e.g. [6]). It is tempting to predict the stability of this mode of operation from the steady state single mode results, but a correct treatment must be based on multimode/multiline calculations. In [4-5] some aspects of line competition have been discussed. In this paper we mainly concentrate on mode competition inside a line. The results can, of course, also be applied to line competition within the simplified three-level scheme used. It is not necessary to assume an off-resonant pump which is only required for clearly distinguishable line center and Raman resonances.

The assumption of a single frequency probe at ν_1 is not fully consistent in the presence of a FIR mode of arbitrary intensity at ν_0, even in the weak probe limit. The reason is that beating of the probe with the strong mode creates a polarization at a frequency $2\nu_0-\nu_1$, i.e. symmetrically to ν_1 with respect to ν_0. This polarization generates an EM field which in turn reacts back via the same mechanism onto the original probe at ν_1. In an exact approach one must employ a bichromatic probe which possesses two frequencies located symmetrically with respect to the main mode. Naturally this situation implies slightly more complicated calculations (e.g., two probe amplitudes occur). Hence it is of interest to investigate the conditions for which the single probe approach is adequate.

The bichromatic probe approach has strongly been inspired by the papers [7-8]. Their formalisms can easily be extended to our three-level system. The mathematical tools required are directly obtainable from the general multimode theory of FIR lasers outlined in [10]. Similarily to [7] we are able to determine the first instability threshold of the full Hopf hierarchy [2]. The instability study is not the primary goal of this paper, but it is of interest to note that the present model takes into account all relevant coherence processes. Hence it is well suited to studying several instability questions in FIR lasers which are perhaps the most promising testbeds of some problems in nonlinear laser dynamics [9].

In section II we shall introduce the theoretical model and the notation in addition to reviewing some basic single mode operation characteristics. In section III we shall calculate the small signal gain spectra in the presence of an intense single mode pump and <u>one</u> arbitrary FIR mode. Both single frequency and bichromatic probes are discussed. Representative probe spectra are analyzed and the validity of the single frequency probe approach will briefly be studied. Section IV is devoted to an exploration of parameter regions where single mode FIR operation is to be expected. Finally section V gives a summary and a discussion of the results.

II. MODEL SYSTEM

A. General Equations

In many cases the simple three-level system shown in Fig. 1 provides an accurate enough approximation for calculating the FIR gain. However, the degeneracy of real molecular levels and the possibility that other levels may also be active (cf. e.g. [5,11]) has to be kept in mind. The classical EM field is composed of a single mode pump (at a frequency Ω), coupling to the transition $1 \to 2$ only, one arbitrarily intense FIR mode (frequency ν_0), and one or two weak FIR side modes (frequencies ν_1 and ν_{-1}) acting as probes. The FIR fields are assumed to be coupled only to the transition $2 \to 3$. To lowest order in the probe amplitudes a probe interaction appears only when the probes are at symmetrical frequencies around ν_0. Sometimes a single probe approach is sufficient (to be discussed more explicitely in section III), but in general one should employ a bichromatic probe. The reason is that after a certain distance of propagation in thick samples an external probe inevitably creates a symmetric side band polarization which induces the corresponding field component pair.

The polarization of the active three-level medium is calculated by semiclassical theory. The existence of three FIR modes calls for numerical techniques developped for multimode or standing wave lasers. We shall employ here the Fourier expansion method of [10]. Also the notation and the method of solution are adapted from that source. Because here we are only interested in the linear response to the probe fields (the pump and one FIR mode remain arbitrary) the infinite Fourier series truncate to a reasonably simple closed set of coupled equations which can also be derived directly without resorting to the full complexity of ref. [10] (see Appendix A). The main approximations of the model include the rotating wave approximation, the assumption of slowly varying field ammplitudes of co-running waves, the neglect of longitudinal and transverse amplitude variations (c.f. the destruction of instabilities by transverse mode structure [12]), utterly simplified collisional and pumping processes, and the approximations connected with the adopted level scheme (neglect of degeneracy, simplified form of the Stark shifts, etc.). Many of these effects can be taken into account, but at the expense of largely increased complexity.

Within the rotating wave approximation (the fast frequency removed is Ω in the case of $1 \leftrightarrow 2$ elements and ν_0 for the $2 \leftrightarrow 3$ transition) the slowly varying density matrix elements ρ_{ij} obey the equations of motion

$$\dot{\rho}_{21} = -(\gamma_{21} + i\Delta_{21})\rho_{21} + i\alpha(\rho_{22} - \rho_{11}) - i\beta\rho_{31} \tag{II.1}$$

$$\dot{\rho}_{23} = -(\gamma_{23} + i\Delta_{23})\rho_{23} + i\beta(\rho_{22} - \rho_{33}) - i\alpha\rho_{31}^{*} \tag{II.2}$$

$$\dot{\rho}_{31} = -(\gamma_{31} + i\Delta_{31})\rho_{31} + i\alpha\rho_{23}^{*} - i\beta^{*}\rho_{21} \tag{II.3}$$

$$\dot{\rho}_{11} = \Gamma_1(\overset{\circ}{n}_1 - \rho_{11}) + 2\,\mathrm{Im}(\alpha^{*}\rho_{21}) \tag{II.4}$$

$$\dot{\rho}_{22} = \Gamma_2(\overset{\circ}{n}_2 - \rho_{22}) - 2\,\mathrm{Im}(\alpha^{*}\rho_{21} + \beta^{*}\rho_{23}) \tag{II.5}$$

$$\dot{\rho}_{33} = \Gamma_3(\overset{\circ}{n}_3 - \rho_{33}) + 2\,\mathrm{Im}(\beta^{*}\rho_{23}) \tag{II.6}$$

and $\rho_{ij} = \rho_{ji}^{*}$.

The complex pump field amplitude E_p which also contains the phase appears in the flipping rate $\alpha=\mu_{21}E_p/2\hbar$ where μ_{21} is the dipole matrix element. The pump detuning enters the factor $\Delta_{21} = \omega_{21}-\Omega$ where ω_{21} is the molecular transition frequency. In the present case the FIR field is composed of three components :

$$\beta = \beta_0+\beta_1 e^{-i\delta_1 t}+\beta_{-1}e^{-i\delta_{-1}t} \tag{II.7}$$

where β_0 is the flipping rate $\beta_0 = \mu_{23}E_0/2\hbar$, due to the arbitrarily intense center mode and $\beta_{\pm 1}$ represent the corresponding probe quantities. The detuning factor $\Delta_{23} = \omega_{23}-\nu_0$ depends on the center mode frequency. The remaining explicit time dependence resides in the exponentials varying at the beat frequencies $\delta_{\pm 1}=\nu_{\pm 1}-\nu_0$. As discussed above we only have to consider either a single frequency probe, i.e. $\beta_{-1}=0$, or a bichromatic probe where $\delta_1=-\delta_{-1}$. In both cases we shall drop the index 1 from the beat frequencies for brevity (i.e. $\delta=\nu_1-\nu_0$ and $\nu_{-1}=\nu_0-\delta$).

Collisional relaxation is taken into account by the damping rates γ_{ij} ($\Gamma_i=\gamma_{ii}$) which in the following are generally assumed to be equal just for mathematical simplicity. Note that keeping the γ_{ij}'s unequal sometimes facilitates the tracing of the origin of various characteristic spectral features and also provides a crude means to simulate field incoherence effects. We will also usually assume that only the lowest level is thermally populated ($n_2^0=n_3^0=0$). This assumption is trivially relaxed.

The general stationary solution of Eqs. (II.1)-(II.6) can be expressed as a Fourier expansion $\sum\rho_{ij}(m)\exp(-im\delta t)$ (one-dimensional when δ_{-1} is a multiple of δ_1) where the expansion coefficents can be obtained by the methods based on matrix continued fractions [10]. The pump and FIR gain factors are related to $\rho_{21}(1)$ and $\rho_{23}(1)$ by

$$G_p = \frac{\Omega \mu_{21}^2}{\hbar \varepsilon_0 c} \operatorname{Im}\left(\rho_{21}(0)/\alpha\right) \tag{II.8}$$

$$G_\ell = \frac{\nu_0 \mu_{23}^2}{\hbar \varepsilon_0 c} \operatorname{Im}\left(\rho_{23}(\ell)/\beta_\ell\right) \qquad (\ell = 0, \pm 1) \tag{II.9}$$

respectively. In the single mode case in the general Fourier series only the components with l=0 are non-vanishing and we recover the familiar single mode intense field FIR results (see e.g. [6]; some characteristics will be briefly reviewed in the next section). The main topic in this paper is, however, the weak probe response for which also $\rho_{23}(\pm 1)$ are non-vanishing (the truncation of the Fourier expansion is described in more detail in appendix A).

B. Single-mode Operation Characteristics

Formulas for obtaining the exact single mode response are given in Appendix A (Eqs (A9)-(A13)). As long as all the FIR modes remain weak, their mutual interaction is negligible and the gain spectrum is given by

$$G_0 = \frac{\nu_0 \mu_{23}^2 n_1^0}{\hbar \varepsilon_0 c} \frac{|\alpha|^2}{\Delta_{21}^2 + \gamma^2 + 4|\alpha|^2} \cdot \operatorname{Re}\left\{ \frac{2(\gamma - i\Delta_{31}) + \gamma + i\Delta_{21}}{(\gamma - i\Delta_{31})(\gamma + i\Delta_{23}) + |\alpha|^2} \right\} \tag{II.10}$$

assuming negligible thermal population of the levels 2 and 3. When we have $(n^0_2 - n^0_3) \neq 0$ a linear term is introduced into the gain which, however, is dominated by the non-linear part (II.10) already at modest values of $|\alpha|^2$. The gain spectrum obtained by varying Δ_{23} (note that $\Delta_{31} = \Delta_{21} - \Delta_{23}$) decomposes into two resonances centered at $\Delta_{23} = \omega_\pm$

$$\omega_\pm = 1/2\ \Delta_{21} \pm \left[1/4\ \Delta_{21}^2 + |\alpha|^2 \right]^{1/2} \tag{II.11}$$

The two peaks are resolved if their separation exceeds their width γ. For equal relaxation rates and negligible Doppler broadening (easy to include; e.g. $\Delta_{21} \rightarrow \Delta_{21} - Kv$), the heights of the two peaks are equal.

One way to interpret (II.10) - (II.11) is based on the dressed atom formalism (for details see e.g. [13] and original references therein). The pump field part of the interaction is diagonalized and the ensuing eigenvalues correspond to (II.11). For a resonant pump $\Delta_{21}=0$, the spectrum (II.10) exhibits symmetric AC Stark splitting with peaks at $\Delta_{23} = \pm\alpha$.

For a detuned pump (take e.g. $\Delta_{21} \gg |\alpha|, \gamma$), the maxima of (II.10) lie at $\omega_+ \approx \alpha^2 / \Delta_{21}$ and $\omega_- \approx -\Delta_{21} - \alpha^2 / \Delta_{21}$ corresponding to AC Stark shifted line center (or laser like) and Raman emission resonance frequencies, respectively. The terminology - line center and Raman resonance - refers to the bare atom picture and is strictly justifiable only in the weak pump limit. To further elucidate this point we solve ρ_{23} in the steady state from (II.2) and get

$$\rho_{23} = \left[i\beta(\rho_{22} - \rho_{33}) - i\alpha\rho_{31}^* \right] / (\gamma_{23} + i\Delta_{23}) \tag{II.12}$$

where the first term in the brackets closely resembles a laser like contribution. In our case the population inversion $\rho_{22}-\rho_{33}$ is only created by the pump :

$$\rho_{22} - \rho_{33} = 2\alpha^2 n_1^0 / \Delta_{21}^2 \qquad \text{(II.13)}$$

The result is valid for $|\Delta_{21}| \gg \gamma > |\alpha|$. The second term in (II.12) represents pure quadruple coherence effects and reduces in the same limit as (II.13) to

$$\rho_{31} = (i\alpha\beta^* n_1^0 / \Delta_{21}) [\gamma_{31} + i(\Delta_{21} - \Delta_{23})]^{-1} \qquad \text{(II.14)}$$

This expression combined with (II.12) yields the familiar formula for the gain of stimulated Raman emission (see e.g. [14], Cpts.7 - 8). The contributions (II.13) and (II.14) are responsible for the line center and Raman resonance, respectively.

The dressed atom formalism is expedient in describing the probe behavior as long as the matter-field interaction contains one strong and one weak part. Hence the method is for instance well suited for the analysis of the probe gain $G(\beta_{\pm 1})$ in the presence of an arbitrary β_0 and α, but is of little use in calculating the gain $G(\beta_0)$ in the region where saturation due to β_0 becomes important. For this reason we do not attempt to label various features of the strong signal gain spectra. The analysis can be based on the rather exhaustive strong signal calculations given e.g. by Panock and Temkin [6].

For the readers' convenience we have reproduced a couple of intense field spectra in Figs. 2 and 3. When the pump is resonant (Fig.2), the AC Stark splitting disappears as β_0 is increased and a strongly saturated singly peaked spectrum results. This phenomenon is usually referred to as power broadening, but actually it is caused by Rabi flipping i.e. its origin is purely dynamic and not an incoherent relaxation. At exact resonance, $\Delta_{21}=\Delta_{23}=0$, the flipping frequency equals $(\alpha^2+\beta_0{}^2)^{1/2}$ which shows that when $\beta_0 \gg \alpha$ the broadening due to β_0 dominates and exactely as in two-level systems the spectrum does show only a single peak.

In the case of off-resonant pumping, Fig.3, the two peaks - Raman and line center - show different saturation behavior. The line center gain is bleached much faster as β_0 is increased. Near the line center the dimensionless saturation parameter is proportional to $\beta_0{}^2/\gamma^2$; near the Raman resonance the corresponding quantity is of the order $\beta_0{}^2\alpha^2/\Delta_{21}{}^2\gamma^2$ which for large pump detunings can be very small (this feature allows to get higher FIR output powers with off-resonant pumping). For very large values of β_0 the two peaks merge together resulting in a skewed singly peaked spectrum. The situation resembles the resonant case (Fig.2), the more the larger β_0 is.

In a self-consistent treatment of an oscillator or an amplifying medium the intensity of the main FIR mode must be determined from its gain. Frequently it is necessary to also consider dispersion. In this paper, however, we will treat both β_0 and ν_0 as free parameters (for an outline of a fully consistent calculation see e.g. cpt. 3 of [15]). Another feature of $G(\beta_0)$ worth mentioning is that for a range of fixed values of Δ_{23} it does not behave monotonically. This enables the occurence of bistability and possible onset of bifurcations.

III. PROBE RESPONSE

A. Single-Mode Probe

We shall first neglect the component β_{-1} in (II.7). In the case of a weak probe β_1 one only has to take into account the components ρ_{ij} (m) with $|m|\leq 1$ in the Fourier-series solution of (II.1)-(II.6) to obtain the material response to order $O(\beta_1)$. The exact two-mode solution valid for arbitrary β_0 and β_1 is obtainable from the results of [10] by changing the level indices $1 \rightleftarrows 3$ and the fields $\alpha \rightleftarrows \beta$ in addition to the trivial changes in the zero-field level populations caused by the interchanging of the levels 1 and 3. The coefficients $\rho_{ij}(0)$ provide the single-mode solution discussed in the previous section (valid for $\beta_1 \to 0$). The first order terms form a set of eight coupled algebraic equations; note that only the population differences $D_{ij}(m)=\rho_{ii}(m)-\rho_{jj}(m)=D_{ij}{}^*(-m)$ are required. Generally the solution has to be done numerically, but in some limiting cases astonishingly simple analytical results are obtainable as shown e.g. in [4] where a detuned pump is assumed. The numerical solution is easily performed and it includes, of course, the intense field effects and is valid for arbitrary detunings within the rotating wave approximation and the validity limits of the simple three-level system. The basic formulas needed are given in Appendix A, Eqs. (A14)-(A21) (note that here we put $\beta_{-1}=0$).

Once the coefficient $\rho_{23}(1)$ is known the probe response is calculated from the non-linear susceptibility χ_1

$$\chi_1 = -\frac{|\mu_{23}|^2}{\hbar\,\varepsilon_0}\;\frac{\rho_{23}(1)}{\beta_1} \tag{III.1}$$

The probe gain (see (II.9)) and dispersion are proportional to $\mathrm{Im}(\chi_1)$ and $\mathrm{Re}(\chi_1)$, respectively. The corresponding properties of the pump and the main FIR mode β_0 are contained in the coefficients $\rho_{21}(0)$ and $\rho_{23}(0)$.

According to (A19) $\rho_{23}(1)$ is composed of three terms

$$\rho_{23}(1) = i\,\mathcal{L}_{23}(1)\cdot$$
$$\cdot\left[\beta_1 D_{23}(0) + \beta_0 D_{23}(1) - \alpha\,\rho_{31}^*(-1)\right] \tag{III.2}$$

where $\mathcal{L}_{23}(1) = [\gamma+i(\omega_{23}-\nu_1)]^{-1}$ (cf. (A8)). The first term is proportional to the DC population difference $[\rho_{22}(0) - \rho_{33}(0)]$ and represents a typical laser like contribution (note that the terminology is not completely unambiguous). It is worth emphasizing that it contains full saturation due to α and β_0 which is also true for the other terms. In the case of an off resonant pump this contribution gives the dominant part of the line center resonance (cf. the discussion in connection with Eq. (II.12)). The third term depending on the quadrupole coherence ρ_{31} is responsible for the two-photon transition $1 \rightarrow (\Omega+\nu_1) \rightarrow 3$ (Raman resonance in the case of detuned pump) exactly as in the single mode case, Eq. (II.12) (in addition it cancels a part of the line center contribution due to $D_{23}(0)$). The second term contains novel effects - population pulsations which are due to mode beating (notice that some beat phenomena enter also via the $\rho_{31}^*(-1)$ term). These population pulsations are exactly analogous to those discussed by Hendow and Sargent [7] in a two-level system (levels 2 and 3 included only). The novel features here are due to the third level 1 which renders possible e.g. the appearence of the quadrupole coherence ρ_{31}.

In Section III.C we shall analyze some representative single mode spectra obtained numerically. Reasonably simple analytical formulas for the probe gain can be derived for instance in the weak pumping limit i.e., when either the pump field is strongly detuned or when its intensity is small enough. Equations valid to order $O(\alpha^2)$ and which also contain all the asymptotic terms to order $O(\Delta_{21}^{-2})$ are given by (A22)-(A27).

As a special case we have calculated the probe response near the line center when the pump is detuned ($|\Delta_{21}| \gg \alpha, \beta_0, \gamma$) and the main FIR mode operates on the Raman resonance. To order $O(\Delta_{21}^{-2})$ we get from (A28)

$$\rho_{23}(1) = i\beta_1 \mathcal{L}_{23}(1)\,\alpha^2 n_1^0 / \Delta_{21}^2 \cdot \left[1 - \beta_0^2/\gamma^2 (2 + \gamma \mathcal{L}_{21}(1)\right] \tag{III.3}$$

where the Lorentzians are generally defined as (cf. (A8)) :

$$\mathcal{L}_{ij}(k) = \left[\gamma_{ij} + i(\Delta_{ij} - k\delta)\right]^{-1} \tag{III.4}$$

Because we have assumed the main mode at Raman resonance, i.e., $\Delta_{23}=\Delta_{21}$, $\mathcal{L}_{23}(1)$ and $\mathcal{L}_{21}(1)$ both are resonant when $\delta=\Delta_{21}$, i.e. when the probe is near the line center. Equation (III.3) does not limit the magnitude of β_0/γ. The quenching of the line center gain as predicted already in [4] is clearly evidenced by (III.3).

If the main FIR mode is at the line center and probing takes place near the Raman resonance, the single probe gain is obtained from (A29) (validity limitations as in (III.3) :

$$\rho_{23}(-1) = i\beta_{-1}\frac{\alpha^2 n_1^0}{\Delta^2}\,\frac{\mathcal{L}_{31}^{*}(1)}{1+\beta_0^2\,\mathcal{L}_{21}^{*}(1)\,\mathcal{L}_{31}^{*}(1)} \qquad \text{(III.5)}$$

For $\Delta_{21}>0$ one must have $\nu_1<\nu_0$ to hit the Raman resonance. One can keep the mode separation δ positive but then the mode β_{-1}, instead of β_1, gives the resonant contribution. According to (III.5), the probe resonance appears at $\nu_{-1}=\nu_0-\Delta_{21}$. When β_0^2 is increased the initial Lorentzian shape deforms into the characteristic split structure of three-level resonances.

Slightly more general expressions corresponding to Eqs. (III.3) and (III.5) are given by (A28) and (A29). For instance in these equations the γ_{ij}'s have been kept distinct which aids in tracing the various contributions. When the probing takes place near the main FIR mode, the accuracy of the single mode approach decreases (cf. (A30) where all FIR modes are assumed near line-center or (A32)-(A33) which is valid for a weak resonant pump and for a resonant β_0). An exception is when the FIR modes are close to the Raman resonance and a detuned pump is used. To order $O(\Delta_{21}^{-2})$ the coupling between the FIR-field components completely disappears as is evident from (A31).

Note, however that the accuracy of (A31) is rather limited and already modest values of β_0 can saturate the gain visibly (cf. Fig.4).

B. Bichromatic Mode

Already in the single probe treatment there appears to order $O(\beta_1)$ a term $\rho_{23}(-1)$ giving rise to a polarization at the frequency $\nu_{-1}=\nu_0-(\nu_1-\nu_0)$. This polarization generates a field β_{-1} which in a general case should be taken into account together with β_1. (Conditions for the validity of the single probe approach will be discussed at the end of this section.) The field β_{-1} reacts back onto β_1, because of symmetry, and therefore the evolution of β_1 and β_{-1} are interdependent.* One has a bichromatic probe (β_1/β_{-1} arbitrary) or for some cases a bichromatic eigenmode of the system (β_1/β_{-1} fixed by the eigenvalue equation, see (III.11), and for more details Appendix B).

The bichromatic probe response is obtained by a simple extension of the single probe theory (all the necessary terms are already contained in the formulas of Appendix A). Instead of (III.1) we now must evaluate the polarization amplitudes from the effective susceptibilities

---

* Note that the terms $\rho_{21}(\pm 1)$ create pump sidebands at frequencies $\Omega\pm(\nu_0-\nu_1)$. This process represents coherent pump scattering from the medium modulated at the beat frequency $\nu_1-\nu_0$. It turns out, however, that generally the pump sidebands will be very efficiently absorbed and they need not to be considered at all.

$$\chi(\nu_{-1}) = \chi_{-1} + \varkappa_{-1}\, \beta_{1}^{*} / \beta_{-1} \qquad \text{(III.6)}$$

$$\chi(\nu_{1}) = \chi_{1} + \varkappa_{1}\, \beta_{-1}^{*} / \beta_{1} \qquad \text{(III.7)}$$

where the self terms $\chi_{\pm 1}$ are as in the single probe case (cf. (III.1)) and formal expressions for the coupling terms $\kappa_{\pm 1}$ are given in Appendix B, Eqs. (B5) and (B7), respectively. Again we would like to point out that the susceptibilities (III.6) and (III.7) contain full saturation due to α and β_0.

Within the slowly varying envelope approximation, the field amplitudes in a resonant cavity are given by (see e.g. [15] cpt.3)

$$\dot{\beta}_n = \left[-\frac{\nu_n}{2Q_n} - i\,(\nu_{cn} - \nu_n) + \tfrac{1}{2}\, i\, \nu_n \chi_n \right] \beta_n \qquad \text{(III.8)}$$

where the first term on the RHS describes cavity losses, ν_{cn} is the cold cavity eigenfrequency of mode n, and the last term is the material contribution. Equation (III.8) is written for a ring cavity for the sake of discussion; the CW amplifier case is completely analogous (change d/dt to cd/dz where c is the speed of light). Self consistency requires that also the main FIR mode obeys (III.8) which determines β_0 and ν_0. We assume that the main mode has practically reached steady state before the probe modes start to develop.

The single mode solution is stable if all side mode fluctuations are damped. According to (III.6)-(III.7) the weak side modes satisfy pairwise the equations

$$\dot{\beta}_{-1} = \left[-\frac{\nu_0}{2Q} - i\left(\nu_{c-1} - \nu_{-1}\right) + \tfrac{1}{2} i \nu_0 \chi_{-1}\right]\beta_{-1} + \tfrac{1}{2} i \nu_0 \varkappa_{-1} \beta_1^* \qquad \text{(III.9)}$$

$$\dot{\beta}_{1} = \left[-\frac{\nu_0}{2Q} - i\left(\nu_{c1} - \nu_{1}\right) + \tfrac{1}{2} i \nu_0 \chi_{1}\right]\beta_{1} + \tfrac{1}{2} i \nu_0 \varkappa_{1} \beta_{-1}^* \qquad \text{(III.10)}$$

where we have put $\nu_n=\nu_0$ in all multiplicative terms. The present situation closely resembles that described in [7-8]. The modes $\{\beta_1, \beta_{-1}\}$ grow and decay together and exhibit an eigenmode pattern.

The characteristic roots of (III.9)-(III.10) are given by

$$\lambda_\pm = -\frac{\nu_0}{2Q} + i\left[\delta_c - \frac{1}{2}\left(\nu_1 - \nu_{-1}\right)\right] + \frac{1}{4} i \nu_0 \left(\chi_{-1} - \chi_1^*\right) \pm \frac{1}{2}\left\{\left[\frac{1}{2} i \nu_0 \left(\chi_{-1} + \chi_1^*\right) - i\left(2\nu_{c0} - \nu_1 - \nu_{-1}\right)\right]^2 + \nu_0^2 \varkappa_{-1} \varkappa_1^*\right\}^{1/2} \qquad \text{(III.11)}$$

where the cold cavity mode spacing $\nu_{c1}-\nu_{c0} = \nu_{c0}-\nu_{c-1}$ is denoted by δ_c and where the oscillation frequency of the center mode is obtained from the condition

$$\nu_0 - \nu_{c0} = -\frac{\nu_0}{2} \mathrm{Re}\left(\chi(\nu_0)\right) \qquad \text{(III.12)}$$

The two roots (III.11) are the complex eigenfrequencies of the bichromatic mode each one giving rise to a corresponding eigenmode. For a special initial value combination $\{\beta_1(0), \beta_{-1}(0)\}$ which happens to match one of the eigenmodes, only one of the exponentials will appear during the temporal evolution of $\{\beta_1(t), \beta_{-1}(t)\}$. If both of the roots $\lambda_\pm$ have negative real parts, any initial fluctuation will damp out and the assumed single mode operation is stable. Otherwise fluctuations at the assumed frequencies ν_1 and ν_{-1} start to grow at linearized growth rates determined by the real parts of (III.11) and with a frequency shift proportional to Re $\chi(\nu_{\pm 1})$. Both eigenmodes may grow i.e. Re$(\lambda_{\pm})>0$, but if one of them has a much larger growth rate or the other one decays, any initial combination of probe mode amplitudes will asymptotically approach the eigenmode structure with the larger growth rate.

Undoubtedly the bichromatic mode treatment is more complicated than the single probe theory and hence it is of interest to study under which conditions the latter proves to be sufficiently accurate. One may also ask if single mode stability analysis gives conservative estimates compared to those performed with bichromatic modes. In other words : does the symmetric probe wave pair aid a weakly damped single mode above oscillation threshold, if the mode is close to it? This is not to be expected if both ν_1 and ν_{-1} lie in the stable region according to the single mode theory. This intuitive statement has to be verified by calculations (next section).

Clearly a single mode approach is adequate if the coupling term $\nu_0{}^2\kappa_{-1}\kappa_1{}^*$ can be neglected in (III.11) or in a thin sample where only β_0 and β_1 are present at the input plane. Throughout the thin sample β_{-1} will remain small compared to the external fields and can be ignored. In the case of an off-resonant pump, which is usually encountered in FIR lasers, one is often considering line interaction effects i.e. the influence of intense Raman oscillation on the line center gain or vice versa. Then the corresponding probe pair ν_{-1} of the line center mode $\nu_1 \approx \omega_{23}$, for example, is far from any atomic resonance (main mode at Raman) and remains negligible (to order $O(\Delta_{21}{}^{-2})$). Generally the probe coupling is roughly measured by the magnitude of β_0/δ which disappears for $\delta \rightarrow \infty$. The coupling may also be ignored if the relative phase angles between β_0 and $\beta_{\pm 1}$ fluctuate rapidly (recall from Appendix B the phase dependence $\kappa_{\pm 1} \sim \beta_0 \beta_0$ of the cross-coupling coefficients) : a measure of the interaction strength in this case would be $\beta_0 \tau_{coh}$ where τ_{coh} stands for a characteristic phase correlation time. A proper quantitative treatment of this situation is beyond the scope of this paper.

C. Representative Gain Spectra

Let us start the discussion by considering single probe gain spectra for a detuned pump and the main FIR mode at the Raman resonance. Fig. 4 shows a typical example with $\Delta_{21} = \Delta_{23} = -4\gamma$. The abcissa is the probe separation from the main FIR mode in units of γ; the value 0 corresponds therefore to Raman resonance and -4 to the position of the line center. The assumed pump amplitude implies that $\alpha/\gamma = 0.1$. In a detuned case (as discussed here) the magnitude of the pump amplitude is not very crucial : an increase in α first introduces visible AC Stark shifts to the Raman and line center resonance positions and once these shifts become comparable with the detunings the spectra start to resemble those observed for a resonant pump (see Fig. 8). In the gain curves of Fig.4 the main FIR mode amplitude β_0/γ increases successively from 0.1 to 5.0. The probe amplitude is kept at $\beta_1 = 0.1\ \gamma$.

At small FIR intensities (curve $\beta_0 = 0.1\gamma$ of Fig.4) the FIR mode interaction is negligible; the gain spectrum reduces to that of Eq. (II.10). Due to a detuned pump the slightly AC Stark shifted Raman and line center resonances are easily recognizable . The shifts are primarily caused by the pump. When β_0 is increased the gain near the line center gets suppressed rather soon, whereas the behaviour near the Raman resonance is much less affected (a considerably larger value of β_0 is required to invert the gain). These features are quantitatively predictable by the formulas (A28) and (A31) within their validity range. From the figure we also note that the simple small signal spectrum becomes heavily distorted and new structures appear as β_0 grows (we shall briefly return to these features at the end of this section).

The single probe approach should be accurate enough in Fig. 4 near the line center (i.e. the region around -4) because there the probe mode separation would be $|\nu_1 - \nu_{-1}| \approx 8\gamma$. This is large enough to validate the neglect of β_{-1} at least for small and intermediate values of β_0 (note that for $\beta_0 \approx 5\gamma$ this is not obvious). The single probe approach should also be reasonably accurate to describe the gain spectrum near the Raman resonance, at least for values of $\beta_0/\gamma < 1$, because the pump is strongly detuned.

Figure 5 displays the two growth rates $\mathrm{Re}\{\lambda_\pm\}$ (see Eq. (III.11)) resulting from a calculation employing a bichromatic probe. The parameters correspond to Fig. 4. The gain curves are now fully symmetric with respect to the Raman resonance (point 0), because for each probe frequency ν_1 there exists the symmetric pair $\nu_{-1} = 2\nu_0 - \nu_1$. For this reason only negative values of δ are displayed. Notice, however, that the actual mode evolution will depend on the eigenmode pattern and its connection to the input values

$\{\beta_1(0), \beta_{-1}(0)\}$. More details concerning the eigenvectors are described in Appendix B. It is also worth mentioning that the branch boundary of the square root of the complex quantities in Eq. (III.11) sometimes introduces a discontinuous change from λ_+ to λ_- and vice versa as δ is varied. In the figures we have eliminated this by continuation. Thus it is no longer possible to make a one-to-one correspondence between the indices of $\lambda_\pm$ in the figures and the signs appearing on the RHS of (III.11).

For small values of β_0, $\mathrm{Re}\{\lambda_+\}$ shows gain in Fig. 5 at both the line center and the Raman resonance. Exactly as in Fig. 4 the line center gain is suppressed as β_0 is increased; the same happens also near the Raman resonance but at higher main FIR mode intensities. The other growth rate $\mathrm{Re}\{\lambda_-\}$, however, seems to remain positive near the Raman resonance (note the rapid suppression near the line center). This implies that in the case of several cavity modes in the Raman region all of them are able to grow. This is in qualitative accordance with the single probe predictions which also indicate gain near the Raman resonance except for $\beta_0/\gamma>1$ where the single probe model is expected to fail.

If the pump intensity is increased the growth rates $\mathrm{Re}\{\lambda_\pm\}$ show more distinct changes than could be anticipated from the single probe results, implying that also the magnitude of α is of central importance in addition to β_0 as regards mode interaction (recall the coupling via ρ_{13} coherences). Fig. 6 shows $\mathrm{Re}\{\lambda_\pm\}$ for $\alpha = 3\gamma$. Due to power shifts the Raman and line center peaks are pushed to about 1.6 γ and -5.6 γ in the single probe spectra (curves not shown). The bichromatic modes have growth rate maxima at $\pm 1.5\gamma$ and $\pm 5.5\gamma$ i.e. still in good agreement with the single probe model. According to Fig. 5 $Re(\lambda_+)$ contains both the line center and the Raman maxima at weak pump intensities, whereas $Re(\lambda_-)$ only shows a prominent Raman gain peak. From Fig. 6 it is apparent that for high pump intensities $Re(\lambda_-)$ dominantly displays "line center resonance structure" (the resonance is heavily modified because $\alpha = 3\gamma$ cf. the discussion in connection with Eq.(II.12)) whereas $Re(\lambda_+)$ seems to repeat the "Raman resonance". Both growth rates turn negative or get at least very strongly saturated for large enough values of β_0. It is also worth noting that $Re(\lambda_+)$ shows a multipeaked structure for large β_0. For instance there appears a shallow but clearly distinguishable extremum at zero probe detuning.

Figures 7 and 8 show the single mode probe spectra for resonant pumps of intensities $\alpha/\gamma = 0.1$ and 3.0, respectively. For a weak pump (Fig. 7), the AC Stark splitting is unresolved. As β_0 is increased the gain spectrum becomes first inverted in the central region and gradually evolves into a two peaked absorption spectrum characterized by the ac Stark splitting due to the main FIR mode. At higher pump levels, Fig. 8, the AC Stark splitting due to α is initially clearly visible and higher values of β_0, as compared to Fig. 7, are required to suppress the gain and turn the spectrum into an AC Stark split (due to β_0) absorption spectrum (the peaks actually occur at $\pm(\alpha^2+\beta_0{}^2)^{1/2}$ as shown below).

Figures 9 and 10 display the growth rates $Re(\lambda_\pm)$ corresponding to the single probe cases of Figs. 7 and 8, respectively. For a weak pump, Fig. 9, both $Re(\lambda_+)$ and $Re(\lambda_-)$ imply appreciable gain near resonant probe tuning. The gain $Re(\lambda_+)$ becomes heavily saturated near $\Delta_{23} \approx 0$ and is inverted in the wings where instead $Re(\lambda_-)$ seems to still provide some amplification (near the line center $Re(\lambda_-)$ gets inverted). The eigenvalue λ_- more clearly repeats the AC Stark split absorption similar to the one appearing in Fig.7.

AC Stark splitting is more pronounced for larger pump intensities, Fig.10. The eigenvalues are nearly degenerate for small β_0, but small differences in them develop at higher values of β_0. As β_0 is increased the original gain maxima at $\pm\alpha$ get pushed around and inverted. Some amplification is still retained both near the line center and far in the wings. Again $Re(\lambda_-)$ contributes more to the wing amplification and $Re(\lambda_+)$ more to the line center gain. Note that this dominance of λ_+ or λ_- determines the eigenmode towards which the probe pattern evolves in the respective frequency range.

The previous figures generally display only the part of the probe spectrum where significant gain or absorption is present. As already mentioned, there appears interesting small scale structure within the figures and also outside the drawn parts. Furthermore we have discussed only two representative combinations of detunings : $\Delta_{21} = \Delta_{23} = -4\gamma$ and $\Delta_{21} = \Delta_{23} = 0$. To obtain an overview of the important tuning regions it is expedient to study the dressed level positions which are given by the roots ω_i of the equation [13]

$$\omega\,(\omega + \Delta_{21})(\omega + \Delta_{23}) - \beta_0^2\,(\omega + \Delta_{21}) - \alpha^2(\omega + \Delta_{23}) = 0 \qquad \text{(III.13)}$$

Probe resonances (both single mode and bichromatic probes) are expected at $\omega_{23} - \nu_{\pm 1} = \pm(\omega_i - \omega_j)$. A particularly important case is the Raman resonance, $\Delta_{21} = \Delta_{23} = \Delta$, where the roots of (III.12) are given by :

$$\begin{aligned} \omega_{1,2} &= -\tfrac{1}{2}\Delta \pm \left(\tfrac{1}{4}\Delta^2 + \alpha^2 + \beta_0^2\right)^{1/2} \\ \omega_3 &= -\Delta \end{aligned} \qquad \text{(III.14)}$$

Some other special cases where the solution of the cubic equation (III.13) is very simple have been listed in [13]. The dressed atom approach readily gives the resonance positions, but more detailed calculations are needed to discuss their actual shape i.e. whether a bump, dip or dispersive curve is manifested. The latter problem is met also in the two probe configurations considered here because in the bichromatic case the interference between the probe components can influence the spectral shape.

To demonstrate the usefulness of Eq. (III.13) we analyse the examples shown in Fig. 11. For instance in Fig. 11a we have $\omega_i/\gamma \approx -15.9, -6.3$ and 12.2 which predict resonances at probe detunings 0, ± 9.6, ± 18.5 and ± 28.1. Most of these are recognizable from the spectrum. In Fig. 11b we have detuned the pump to match $\Delta_{23} = 10\gamma$. The roots are now -19.0, -10.0 and 9.0, giving resonances at 0, ± 9.0, ± 19.0, ± 27.9. The resonance structure at detunings -9.0 and 19.0 is not visible demonstrating the applicability restrictions of (III.13) discussed above. All other resonances are easily recognizable from the figure. Finally in Fig. 11c, full resonance is assumed i.e. $\Delta_{21} = \Delta_{23} = 0$ (note the simple form (III.14) now attains : $\omega_{1,2} = \pm(\alpha^2+\beta_0^2)^{1/2}$ and $\omega_3 = 0$. The expected resonances are at 0,

± 9.4 and ± 18.8 whereby the outer ones manifest themselves as dispersive features according to Fig. 11c. It is worth repeating that the resonance positions are unaffected by the assumed probe configuration. The dressed levels, Eq. (III.13), are entirely determined by the intense field parameters.

IV REGIONS OF SINGLE MODE STABILITY

As discussed earlier, single mode laser operation is unstable if a cavity side mode sees gain in the presence of the oscillating main mode. Side modes separated from the main mode by the intermode frequency δ then develop with two individual slightly shifted wavelengths or sometimes exactly at the same wavelength as the main mode. The latter special case occurs if anomalous dispersion due to the main mode compensates the side-mode frequency offsets (for more details on this subject the reader should consult [7]). The condition for positive gain simply implies that in (III.11) we must have $Re(\lambda_{\pm})>0$ for at least one of the caracteristic roots for either type of sidemode instability to occur. In the case of the one wavelength instability an additional condition, $Im\ (\lambda_{\pm}) = 0$, has to be met so that frequency shifts will be eliminated. The graphic method proposed by Hendow and Sargent [7] can be used to test the two conditions.

The anomalous dispersion which favours the one wavelength instability is related to the gain spectrum consisting of two peaks positioned symmetrically around the single mode oscillation. The shape of the dispersion curves can be deduced qualitatively from the gain curves in analogy to the application of the Kramers - Kronig relations in the linear response theory. Although generally we have not shown the curves $\mathrm{Im}(\lambda_\pm)$, (an example is shown in Fig. 11a) we want to point out that dispersion is trivial to take into account in numerical work.

The onset of instability can be analysed by means of contour line plots of the gain as function of some of the variable parameters. The space of free parameters α, β_0, Δ_{21}, Δ_{23} is four dimensional and hence will not be scanned extensively. With the contour lines in the (β_0, ν_1) plane as shown in Fig. 12 the stability regions, defined by

$(C=\gamma_{23}\hbar\varepsilon_0/\mu_{23}{}^2 n_1{}^0)$

$$\mathrm{Im}\left\{\frac{\gamma_{23}\,\rho_{23}(1)}{n_1^0/\beta_1}\right\} < \frac{C}{Q} \qquad \text{(VI.1)}$$

in the monochromatic case and by the condition $\mathrm{Re}(\lambda_\pm)<0$ in the bichromatic case, can easily be found. Fig. 12 represents a typical case for resonant pumping at medium intensity, whereas Figs 13 and 14 demonstrate the effect of varying the intensity of an off-resonant pump beam. The hatched region in Fig. 14 is the unstable region for a cavity where for the sake of discussion we have arbitrarily chosen the value C/Q = 0.02 for passive losses. The depression created near the line center by the intense Raman oscillation is quite evident from Fig.13 as well as the effect of the dynamic Stark shifts (the broken lines in Figs 12 - 14 represent the resonances predicted by (III.13)).

Despite the fact that the theory discussed in this section is not fully self-consistent for the probe modes (dispersion neglected) and that the temporal evolution has not been studied, it is instructive to apply it to try to interpret the low-level gain spectrum measured in a D_2O laser by Woskoboinikow et al. [1]. In that paper the results have been discussed in terms of the gain spectrum of one intense FIR mode (the main mode β_0). In the light of the present theory it is not surprising that the authors found several inconsistencies. The low-level broadening of the FIR spectrum is mainly due to amplified spontaneous emission inside the cavity and thus it rather reflects the gain spectra of weak probes. For an off-resonantly pumped case at intermediate intensities a symmetrically broadened gain spectrum was observed which, as noted by the authors, does not agree with theory predicting an asymmetric broadening towards line-center. The gain of the intense mode certainly has this asymmetric characteristic, but one should use instead the bichromatic probe gain spectra which apparently are symmetric, as demonstrated above. A quantitative calculation, however, requires also consideration of the eigenmode structure before definite conclusions about the symmetry can be made (notice that both modes will be excited initially because of the broadband spontaneous source term). It has also been noted in [1] that the measured Stark broadening was four times larger than predicted. The authors assumed that hot spots inside the cavity are responsible for this behaviour. However, according to Eq. (III.14) the displacement of the peaks by the dynamic Stark effect is a function of $(\alpha^2 + \beta_0^2)$ if $\Delta_{21} = \Delta_{23}$. Hence both the pump and the intense FIR field act in the same way and, perhaps, it is not necessary to invoke hot spots to explain the observed shifts.

An interesting observation in this context is the fact that our theory predicts negative or at least greatly reduced probe gain practically everywhere for sufficiently intense FIR fields. It should be possible to reduce significantly the low level linewidth by operating in this regime. This has not to our knowledge been tested experimentally for the simple reason that the output coupling would have to be far from optimum to reach such a highly saturated regime.

V. SUMMARY AND DISCUSSION

Single mode operation is a prerequisite for a great range of laser applications. This is also true for optically pumped FIR lasers which have been developped to produce high power output for specific applications such as collective Thomson scattering to measure the ion temperature in fusion plasmas. In this particular context an emission bandwidth which remains narrow down to very low signal levels is required to alleviate interference of parasitic stray light with the spectrally broadened scattered signal of a level of the order of 10^{-14} times the incident intensity. If lossy mode-selective elements are to be avoided in the resonator, single mode pumping has been found to be essential for the achievement of single mode FIR operation. Pulsed FIR lasers are often pumped off-resonantly and hence capable of emitting radiation on line center or at the Raman shifted frequency. In a previous paper [4] we have shown that line center emission is usually efficiently suppressed already by a moderately intense Raman field. This is certainly the case in three level systems, whereas a more complicated situation arises if additional levels are optically coupled with the pump or FIR fields [5].

For high-power applications long resonators with closely spaced axial modes are often used. This has given the main impetus for the calculations of the present paper where the competition of modes within the gain bands of individual lines and the stability of single mode operation are the central theme.

Single mode theories which are reviewed in chapter II have occasionally been used in the past to interpret experimental results on stability and mode competition. The inadequacy of this approach is clearly demonstrated in chapter III which discusses representative gain spectra for single mode and bichromatic probes. In both approaches, the probe spectra have completely different behaviour from that of the main mode already at moderate intensities α^2 and $\beta_0{}^2$. It has been found that the simpler single mode probe approach is adequate to investigate line competition effects or the competition of modes which are sufficiently off-set from the main FIR mode. Bichromatic probe modes, however, are usually required to study the interaction of modes within the same line. Exceptions to this include for instance Raman modes for a strongly detuned pump and a case where the pump phase varies rapidly enough to cause the decoupling of the bichromatic mode components.

The dressed atom formalism is shown to be very useful for predicting resonances in the probe spectra. Particularly simple expressions are obtained for the Raman resonances which are often encountered in practice. In a most general case the probe spectra display seven resonance positions.

In Chapter IV regions of stable single mode operation have been exemplified. Even without extensive calculations the present theory enabled us to speculate about two previously unexplained observations concerning the low-level linewidth of a D_2O laser. A proposition to reduce this low-level bandwidth has been made. Clearly further investigations and parameter explorations are needed to understand all the details of single mode stability.

The present theoretical model contains several simplifying approximation which must be reconsidered when applying the results to specific experiments. In an attempt to simulate the behaviour of an off-resonantly pumped D_2O laser at 385μm used in our laboratory, we coupled our stability analysis code to a code based on rate type equations which was developped to predict the pulse shape and saturation behavior of the laser [16]. Based on the values of $\alpha(t)$, $\beta_0(t)$, and the equilibrium populations calculated by the rate equation code, the tendency for multimode operation was obtained for every chosen timestep. For the case of the ring laser developped at UCLA [17] or the Fabry-Perot system in our laboratory the numerical results predict a tendency for multimode operation at high pressures (> 5 torr) because of the decreasing ratio of β_0/α and the increasing homogeneous line width. This contradicts experimental findings where single mode operation becomes easier to achieve at higher pressures. Evidently certain assumptions of our model are too restrictive. The neglect of transverse or axial effects (cf. [12]) or degeneracy and/or the grossly oversimplified collisional picture may be responsible for this. It is also important to recall that the present calculation assumes adiabaticity i.e. the polarization is expected to have reached a steady state (cf. the clearly different temporal behavior of Raman and line center signals occuring in the optical region [18]). The influence of inhomogeneous broadening, on the other hand is not of significance since this effect was included in our simulations.

Although the present treatment is mainly devoted to studying single mode stability and not to an investigation of the behavior of laser instabilities, we shall finally briefly comment on one question belonging to the latter category : what are the basic differences between a three-level system pumped with a coherent optical source as discussed in the present paper and an ordinary two-level system where the population inversion is created by incoherent pumping. A comparison of spectral shapes shown here and in [7] should provide some answers and enable the reader to find out the most prominent features of the two systems. One obvious difference between the two and three level systems is the quadrupole coherence ρ_{13} which vanishes if the levels 1 and 2 are coupled by an incoherent source. This term is responsible i.a., for stimulated Raman scattering - no corresponding resonance appears in two level systems at large detunings. Another characteristic feature is the AC Stark splitting or shifting due to the pump. Our model reduces exactly to that of [7] if we let $\alpha \to 0$ and choose $n_2^0 - n_3^0 \neq 0$. Formally the same population inversion can be created with a pump intensity $\alpha^2 = (n_2^0 - n_1^0) / (2n_1^0) \cdot \gamma_{21}\Gamma_2$.

AC Stark effects disappear when we let γ_{13} or $\Delta_{13} \to \infty$ i.e., we neglect the Raman resonance.

Acknowledgment : This work has been partially supported by the Swiss National Science Foundation.

REFERENCES

[1] P. Woskoboinikow, W.J. Mulligan, and R. Erickson, "385 μm D_2O laser linewidth measurements to -60 dB" IEEE J. Quantum Electron., vol. QE-19, p. 4-7, 1983.

[2] L.A. Lugiato, L.M. Narducci, D.K. Bandy, and N.B. Abraham, "Instabilities in inhomogeneously broadened single-mode lasers", Opt. Commun., vol. 46, p. 115-120, 1983.

[3] M. Lefebvre, D. Dangoisse, and P. Glorieux, "Transients in a far-infrared laser", Phys. Rev. A., vol. 29, p.758-767, 1984.

[4] M.A. Dupertuis, M.R. Siegrist, and R.R.E. Salomaa, "Competition between Raman and line-center oscillations in optically pumped far-infrared lasers", Phys. Rev. A., vol. 30, p.2824-2826, 1984.

[5] M.A. Dupertuis, R.R.E. Salomaa, and M.R. Siegrist, "Raman and line centre oscillation selection in coherently pumped four-level FIR lasers", Opt. Commun., vol. 54, p. 27-32, 1985.

[6a] R.L. Panock and R.J. Temkin, "Interaction of two laser fields with a three level molecular system", IEEE J. Quantum Electron., vol. QE-13, p.425-434, 1977.

[6b] T.A. De Temple, "Pulsed optically pumped far infrared lasers", Infrared and Millimeter waves, vol. 1, p. 129-184, Ed. K.J. Button, Academic, New-York, 1979.

[7a] S.T. Hendow and M. Sargent III, "The role of population pulsations in single mode laser instabilities", Opt. Commun., vol. 40, p. 385-390, 1982.

[7b] S.T. Hendow and M. Sargent III, "Effects of detuning on single mode laser instabilities", Opt. Commun., vol. 43, p.59-63, 1982.

[8] L.W. Hillman, R.W. Boyd, and C.R. Stroud Jr., "Natural modes for the analysis of optical bistability and laser instability", Opt. lett., vol. 7, p.426-428, 1982.

[9] C.O. Weiss and W. Klische, "On observability of Lorentz instabilities in lasers", Opt. Commun., vol. 51, p.47-48, 1984.

[10] M.A. Dupertuis, R.R.E. Salomaa, and M.R. Siegrist, "Two mode optical pumping of a laser", IEEE J. Quantum Electron., vol. QE-20, p.440-449, 1984.

[11] G. Dodel and N.G. Douglas, "Investigation of D_2O laser emission at 50, 66, 83, 111 and 116 μm", IEEE J. Quantum Electron., vol. QE-18, p. 1294-1301, 1982.

[12] L.A. Lugiato and M. Milani, "Disappearence of laser instabilities in a Gaussian cavity mode", Opt. Commun., vol. 46, p. 57-60, 1983.

[13] P.R. Berman and R. Salomaa, "Comparison between dressed-atom and bare-atom pictures in laser spectroscopy", Phys. Rev. A, vol. 25, p.2667-2692, 1982.

[14] D. Marcuse, Principles of Quantum Electronics, Academic, New York, 1980.

[15] S. Stenholm, Foundations of Laser Spectroscopy, Wiley, New York, 1984.

[16] T. Okada, R. Behn, M.A. Dupertuis, P.D. Morgan and M.R. Siegrist, "Numerical analysis of an optically pumped D_2O far infrared laser", J. Appl. Phys., vol. 54, p.2987-2994, 1983.

[17] W.A. Peebles, D. Umstadter, D.L. Brower and N.C. Luhmann Jr., "A unidirectional, pulsed far infrared ring laser", Appl. Phys. Lett., vol. 38, p.851-853, 1981.

[18] A. Guzman de Garcia, P. Meystre and R.R.E. Salomaa, "Time-delayed probe spectroscopy in two-photon-pumped systems", Phys. Rev. A., vol. 32, p.1531-1540, 1985.

APPENDIX A : Probe response

Inserting the Fourier-expansions $\rho_{ij} = \sum \rho_{ij}(m)\exp(-im\delta t)$ into (II.1) - (II.6) and assuming in (II.7) that $\delta_1 = -\delta_{-1} = \delta$, we get

$$\rho_{21}(k) = i\mathcal{L}_{21}(k)[\alpha D_{21}(k) - \beta_0 \rho_{31}(k) - \beta_1 \rho_{31}(k-1) - \beta_{-1}\rho_{31}(k+1)] \quad \text{(A1)}$$

$$\rho_{23}(k) = i\mathcal{L}_{23}(k)[\beta_0 D_{23}(k) + \beta_1 D_{23}(k-1) + \beta_{-1} D_{23}(k+1) - \alpha \rho_{31}^*(-k)] \quad \text{(A2)}$$

$$\rho_{31}(k) = i\mathcal{L}_{31}(k)[\alpha \rho_{23}^*(-k) - \beta_0^* \rho_{21}(k) - \beta_1^* \rho_{21}(k+1) - \beta_{-1}^* \rho_{21}(k-1)] \quad \text{(A3)}$$

$$(\Gamma_1 - ik\delta)\rho_{11}(k) = \Gamma_1 n_1^0 \delta_{k,0} - i[\alpha^* \rho_{21}(k) - \alpha \rho_{21}^*(-k)] \quad \text{(A4)}$$

$$(\Gamma_2 - ik\delta)\rho_{22}(k) = \Gamma_2 n_2^0 \delta_{k,0} + i[\alpha^* \rho_{21}(k) - \alpha \rho_{21}^*(-k)] + i[\beta_0^* \rho_{23}(k) - \beta_0 \rho_{23}^*(-k) + \beta_1^* \rho_{23}(k+1) - \beta_1 \rho_{23}^*(1-k) + \beta_{-1}^* \rho_{23}(k-1) - \beta_{-1}\rho_{23}^*(-1-k)] \quad \text{(A5)}$$

$$(\Gamma_3 - ik\delta)\rho_{33}(k) = \Gamma_3 n_3^0 \delta_{k,0} - i[\beta_0^* \rho_{23}(k) - \beta_0 \rho_{23}^*(-k) + \beta_1^* \rho_{23}(k+1) - \beta_1 \rho_{23}^*(1-k) + \beta_{-1}^* \rho_{23}(k-1) - \beta_{-1}\rho_{23}^*(-1-k)] \quad \text{(A6)}$$

where D_{ij} is the population difference

$$D_{ij}(k) = \rho_{ii}(k) - \rho_{jj}(k) \quad \text{(A7)}$$

and the complex Lorentzians are defined by

$$\mathcal{L}_{ij}(k) = [\gamma_{ij} + i(\Delta_{ij} - k\delta)]^{-1} \quad \text{(A8)}$$

For arbitrary intensities $\{\alpha, \beta_i\}$ Eqs (A1)-(A6) form an infinite set which can be solved e.g. with the technique used in ref. [10]. For weak $\beta_{\pm 1}$ the perturbation method described below is applicable.

When we have $\beta_{\pm 1} = 0$ only the Fourier-coefficients with an index k = 0 are non-vanishing :

$$\rho_{21}(0) = i\,\mathcal{L}_{21}(0)\left[\alpha D_{21}(0) - \beta_0 \rho_{31}(0)\right] \tag{A9}$$

$$\rho_{23}(0) = i\,\mathcal{L}_{23}(0)\left[\beta_0 D_{23}(0) - \alpha \rho_{31}^*(0)\right] \tag{A10}$$

$$\rho_{31}(0) = i\,\mathcal{L}_{31}(0)\left[\alpha \rho_{23}^*(0) - \beta_0^* \rho_{21}(0)\right] \tag{A11}$$

$$\Gamma D_{21}(0) = -\Gamma n_1^0 - 4\,\mathrm{Im}\left(\alpha^* \rho_{21}(0)\right) - 2\,\mathrm{Im}\left(\beta_0^* \rho_{23}(0)\right) \tag{A12}$$

$$\Gamma D_{23}(0) = -2\,\mathrm{Im}\left(\alpha^* \rho_{21}(0)\right) - 4\,\mathrm{Im}\left(\beta_0^* \rho_{23}(0)\right) \tag{A13}$$

Just for the simplicity of notation we have assumed $\Gamma_i = \Gamma$ (i = 1, 2, 3) and $n_2{}^0 = n_3{}^0 = 0$ in (A12)-(A13).

The first order terms in $\beta_{\pm 1}$ are those with an index k = ±1 :

$$\rho_{21}(1) = i\,\mathcal{L}_{21}(1)\left[\alpha D_{21}(1) - \beta_0 \rho_{31}(1) - \beta_1 \rho_{31}(0)\right] \tag{A14}$$

$$\rho_{31}(1) = i\,\mathcal{L}_{31}(1)\left[\alpha \rho_{23}^*(-1) - \beta_0^* \rho_{21}(1) - \beta_{-1}^* \rho_{21}(0)\right] \tag{A15}$$

$$\rho_{23}^*(-1) = -i\,\mathcal{L}_{23}^*(-1)\left[\beta_0^* D_{23}(1) + \beta_{-1}^* D_{23}(0) - \alpha^* \rho_{31}(1)\right] \tag{A16}$$

$$\rho_{21}^{*}(-1) = -i\mathcal{L}_{21}^{*}(-1)\left[\alpha^{*} D_{21}(1) - \beta_{0}^{*}\rho_{31}^{*}(-1) - \beta_{-1}^{*}\rho_{31}^{*}(0)\right] \tag{A17}$$

$$\rho_{31}^{*}(-1) = -i\mathcal{L}_{31}^{*}(-1)\left[\alpha^{*}\rho_{23}(1) - \beta_{0}\rho_{21}^{*}(-1) - \beta_{1}\rho_{21}^{*}(0)\right] \tag{A18}$$

$$\rho_{23}(1) = i\mathcal{L}_{23}(1)\left[\beta_{0} D_{23}(1) + \beta_{1} D_{23}(0) - \alpha\rho_{31}^{*}(-1)\right] \tag{A19}$$

$$(\Gamma - i\delta) D_{21}(1) = 2i\left[\alpha^{*}\rho_{21}(1) - \alpha\rho_{21}^{*}(-1)\right] + i\left[\beta_{0}^{*}\rho_{23}(1) - \beta_{0}\rho_{23}^{*}(-1) - \beta_{1}\rho_{23}^{*}(0) + \beta_{-1}^{*}\rho_{23}(0)\right] \tag{A20}$$

$$(\Gamma - i\delta) D_{23}(1) = i\left[\alpha^{*}\rho_{21}(1) - \alpha\rho_{21}^{*}(-1)\right] + 2i\left[\beta_{0}^{*}\rho_{23}(1) - \beta_{0}\rho_{23}^{*}(-1) - \beta_{1}\rho_{23}^{*}(0) + \beta_{-1}^{*}\rho_{23}(0)\right] \tag{A21}$$

Note that we have $D_{ij}(-k) = D_{ij}^{*}(k)$. The zeroth order solution given by (A9)-(A13) appears above in the inhomogeneous terms. Generally it is preferable to solve (A14)-(A21) numerically. Only in some particular cases reasonably simple and informative expressions for $\rho_{23}(\pm 1)$ are obtainable : e.g. when the pump is strongly detuned (cf. [4-5]) or when all the FIR-modes are weak (cf. Eq. (II.10]).

Many interesting features of the system can be predicted by a weak pumping model which is valid when either α is small or Δ_{21} is large. To order $O(\alpha^2)$ we get from (A9)-(A21)

$$\rho_{23}(1) = i\mathcal{L}_{23}(1)\{\beta_1 D_{23}(0) + \beta_0 D_{23}(1) - [i\alpha\rho_{21}^*(0)\mathcal{L}_{31}^*(-1)]/[1+\beta_0^2\mathcal{L}_{21}^*(-1)\mathcal{L}_{31}^*(-1)] \cdot [\beta_1 - \beta_{-1}^*\beta_0\beta_0\mathcal{L}_{21}^*(-1)\mathcal{L}_{31}^*(0)]\} \tag{A22}$$

$$\rho_{23}(-1) = i\mathcal{L}_{23}(-1)\{\beta_{-1} D_{23}(0) + \beta_0 D_{23}^*(1) - [i\alpha\rho_{21}^*(0)\mathcal{L}_{31}^*(1)]/[1+\beta_0^2\mathcal{L}_{21}^*(1)\mathcal{L}_{31}^*(1)] \cdot [\beta_{-1} - \beta_1^*\beta_0\beta_0\mathcal{L}_{21}^*(1)\mathcal{L}_{31}^*(0)]\} \tag{A23}$$

$$(\Gamma - i\delta)D_{23}(1) = -i\alpha^*\mathcal{L}_{21}(1)\rho_{21}(0)[\beta_1\beta_0^*\mathcal{L}_{31}(0) + \beta_{-1}^*\beta_0\mathcal{L}_{31}(1)] [1+\beta_0^2\mathcal{L}_{21}(1)\mathcal{L}_{31}(1)]^{-1} + i\alpha\mathcal{L}_{21}^*(-1)\rho_{21}^*(0) [\beta_{-1}^*\beta_0\mathcal{L}_{31}^*(0) + \beta_1\beta_0^*\mathcal{L}_{31}^*(-1)]\cdot[1+\beta_0^2\mathcal{L}_{21}^*(-1)\mathcal{L}_{31}^*(-1)]^{-1} + 2i[\beta_0^*\rho_{23}(1) - \beta_0\rho_{23}^*(-1) - \beta_1\rho_{23}^*(0) + \beta_{-1}^*\rho_{23}(0)] \tag{A24}$$

In (A22)-(A24) we have written $\beta_0\beta_0$ explicitly to distinguish it from $\beta_0{}^2 = |\beta_0|^2$. The source terms needed in (A22)-(A24) read

$$\rho_{21}(0) = -i\alpha\mathcal{L}_{21}(0)n_1^0/[1+\beta_0^2\mathcal{L}_{21}(0)\mathcal{L}_{31}(0)] \tag{A25}$$

$$D_{23}(0) = 2\alpha^2 n_1^0/[\Gamma + 4\beta_0^2\,\mathrm{Re}\{\mathcal{L}_{23}(0)\}] \cdot \mathrm{Re}\{\mathcal{L}_{21}(0)[1-2\beta_0^2\mathcal{L}_{23}^*(0)\mathcal{L}_{31}(0)]/ [1+\beta_0^2\mathcal{L}_{21}(0)\mathcal{L}_{31}(0)]\} \tag{A26}$$

$$\rho_{23}(0) = i\beta_0\mathcal{L}_{23}(0)[D_{23}(0) + \{\alpha^2\mathcal{L}_{31}^*(0)\mathcal{L}_{21}^*(0)n_1^0\}/\{1+\beta_0^2\mathcal{L}_{21}^*(0)\mathcal{L}_{31}^*(0)\}] \tag{A27}$$

Considerable further simplification occurs when some of the fields are detuned. Note that all terms to order $O(\Delta_{21}{}^{-2})$ are present in (A22)-(A27). Some example cases are worked out below.

Let us first assume a detuned pump ($\Delta_{21} = \Delta$) and the main FIR-mode at Raman resonance ($\Delta_{23} = \Delta$). If the probe is near the line-center i.e. $\delta \simeq \Delta$ the near resonant Lorentzians in (A22)-(A27) are $\mathcal{L}_{21}(1)$, $\mathcal{L}_{23}(1)$ and $\mathcal{L}_{31}(0)$. Since $\rho_{23}(0)$ and $D_{23}(0)$ are of the order $O(\Delta^{-2})$ and $\rho_{21}(0)$ of the order $O(\Delta^{-1})$ one obtains to order $O(\Delta^{-2})$ from (A22)-(A27).

$$\rho_{23}(1) = i\beta_1 \mathcal{L}_{23}(1)\, \alpha^2 n_1^0 / \Delta^2 \cdot \left[2\gamma_{21}/\Gamma - 1 - \beta_0^2/\gamma_{31}\left(2/\Gamma + \mathcal{L}_{21}(1)\right)\right] \qquad \text{(A28)}$$

From (A28) one easily derives with the aid of (II.9) the probe gain. The result is a slightly generalized form of that given in [4] (recall, however, the limit $\beta_1 \to 0$ assumed here). As now $\rho_{23}(-1)$ is of the order $O(|\Delta_{21}{}^{-3}|)$ a single mode probe is sufficient.

If the main mode is at line center and the probing takes place near the Raman resonance the Lorentzians close to resonance are $\mathcal{L}_{21}(1)$, $\mathcal{L}_{23}(0)$ and $\mathcal{L}_{31}(1)$. The probe gain is now obtained from (A23) :

$$\rho_{23}(-1) = i\beta_{-1}\, \alpha^2 n_1^0 / \Delta^2 \cdot \mathcal{L}_{31}^*(1) \left[1 + \beta_0^2 \mathcal{L}_{21}^*(1)\, \mathcal{L}_{31}^*(1)\right]^{-1} \qquad \text{(A29)}$$

which is in full agreement with [4]. (Notice that because one usually implicitly chooses $\delta > 0$ and $\Delta > 0$, the indexing of the probe changes from

β_1 to β_{-1} when the probe frequency becomes smaller than that of the main mode. The situation reverses for $\Delta<0$. One could equally well let δ be negative in which case the probe gain would follow from (A22) with $\mathcal{L}_{31}{}^*(-1)$ being a resonant Lorentzian for $\delta\simeq-\Delta$.)

If the probes are under the same line as the main mode usually both β_1 and β_{-1} contribute. When all the FIR modes are near the line-center, i.e. the Lorenzians $\mathcal{L}_{23}(k)$ $(k=0,\pm1)$ are the resonant ones, we get for off-resonant pumping (notice that $|\delta|\ll\Delta$) :

$$\rho_{23}(1)=\frac{i\alpha^2 n_1^0\,(2\gamma_{21}/\Gamma-1)\,\mathcal{L}_{23}(1)}{\Delta^2\left[1+(4\beta_0^2/\Gamma)\,\mathrm{Re}\,\mathcal{L}_{23}(0)\right)}$$

$$\left\{\beta_1-2\beta_0\frac{\beta_1\beta_0^*\left[\mathcal{L}_{23}(1)+\mathcal{L}_{23}^*(0)\right]+\beta_0\beta_{-1}^*\left[\mathcal{L}_{23}^*(-1)+\mathcal{L}_{23}(0)\right]}{\Gamma-i\delta+2\beta_0^2\left[\mathcal{L}_{23}(1)+\mathcal{L}_{23}^*(-1)\right]}\right. \tag{A30}$$

The expression for $\rho_{23}(-1)$ is obtained from above by interchanging the indices $+1 \leftrightarrow -1$ in the flipping frequencies β_i and by replacing δ by $-\delta$. Notice in (A30) the full saturation due to the main mode and the probe coupling introduced by the term proportional to $\beta_0\beta_0\beta_{-1}^*$. The only trace of the ρ_{31}-coherence is the factor -1 in the term $(2\gamma_{21}/\Gamma-1)$.

If all the FIR modes are near the Raman resonance we get for off-resonant pumping

$$\rho_{23}(\pm1)=i\alpha^2 n_1^0/\Delta^2\cdot\beta_{\pm1}\,\mathcal{L}_{31}^*(\mp1) \tag{A31}$$

To order $O(\Delta^{-2})$ the modes do not interact at all. Furthermore, the main mode does not introduce any saturation. We point out, however, that this approximation has a rather limited validity range as is evidenced, e.g. by Fig. 5.

As a final example we consider the case where both the pump and the main FIR mode are tuned to exact resonance. To order $O(\alpha^2)$ we get

$$\rho_{23}(1) = \frac{i\mathcal{L}_{23}(1)\alpha^2 n_1^0}{\gamma_{21}\gamma_{31}+\beta_0^2} \tag{A32}$$

$$\left\{\beta_1 \frac{2\gamma_{23}\gamma_{31}-4\beta_0^2}{\Gamma\gamma_{23}+4\beta_0^2} + \frac{\beta_0(\beta_1\beta_0^*+\beta_{-1}\beta_0)\kappa(1)}{\Gamma-i\delta+4\beta_0^2\mathcal{L}_{23}(1)}\right.$$

$$\left.+\frac{\mathcal{L}_{31}(1)}{1+\beta_0^2\mathcal{L}_{21}(1)\mathcal{L}_{31}(1)}\left[\gamma_{31}\beta_1-\beta_{-1}^*\beta_0\beta_0\mathcal{L}_{21}(1)\right]\right\}$$

where $\kappa(1)$ is defined as

$$\kappa(1) = 4\mathcal{L}_{23}(1) - 2(\Gamma+2\gamma_{31})(1+\gamma_{23}\mathcal{L}_{23}(1))/(\Gamma\gamma_{23}+4\beta_0^2)$$

$$-[\mathcal{L}_{21}(1)+2\mathcal{L}_{23}(1)][1+\gamma_{31}\mathcal{L}_{31}(1)]/ \tag{A33}$$

$$(1+\beta_0^2\mathcal{L}_{21}(1)\mathcal{L}_{31}(1))$$

In (A32) the first term in the traces arises from $D_{23}(0)$, the second one from $D_{23}(1)$ and the last one from the quadrupole coherence ρ_{31} (cf., (A22)). We obtain an expression for $\rho_{23}(-1)$ by interchanging the indices $1 \leftrightarrow -1$ and replacing δ by $-\delta$. In the limit $\gamma_{31} \to \infty$

(A32)-(A33) reproduce the probe gain in a two-level system with an effective upper level population $2\alpha^2 n_1{}^0/\gamma_{21}\Gamma$:

$$\rho_{23}(1) = \frac{2i\alpha^2 n_1^0 \mathcal{L}_{23}(1)}{\gamma_{21}\Gamma(1+4\beta_0^2/\gamma_{23}\Gamma)} \Big\{ \beta_1 \tag{A34}$$

$$- 2\beta_0(\beta_1\beta_0^* + \beta_{-1}\beta_0)(1+\gamma_{23}\mathcal{L}_{23}(1))\left[\gamma_{23}(\Gamma - i\delta + 4\beta_0^2\mathcal{L}_{23}(1))\right]^{-1}\Big\}$$

This expression is the same as the one given in [7].

APPENDIX B : Bichromatic probing

Let us define a vector $\bar{R}$ whose components R(i) for i = 1 to 8 are $\rho_{23}(1)$, $\rho_{21}^*(-1)$, $\rho_{31}^*(-1)$, $\rho_{23}^*(-1)$, $\rho_{21}(1)$, $\rho_{31}(1)$, $D_{21}(1)$ and $D_{23}(1)$ in respective order. Eqs (A14)-(A21) can then be rewritten in the compact form

$$\underline{\underline{A}}\,\bar{R} = \beta_1 \bar{S}_1 + \beta_{-1}^* \bar{S}_{-1}^* \tag{B1}$$

Where the 8 × 8 matrix $\underline{\underline{A}}$ and the source vectors $\bar{S}_{\pm 1}$ are easily obtainable from the original equations. After inverting (B1) we get the expressions

$$\rho_{23}(1) = \sum_{k=1}^{8} A_{1k}^{-1}\left[\beta_1 S_1(k) + \beta_{-1}^* S_{-1}^*(k)\right] \tag{B2}$$

$$\rho_{23}(-1) = \sum_{k=1}^{8} (A_{4k}^{-1})^*\left[\beta_1^* S_1^*(k) + \beta_{-1} S_{-1}(k)\right] \tag{B3}$$

for the off-diagonal density matrix elements $\rho_{23}(\pm 1)$ required when calculating the polarization at the probe frequencies. From (III.1), (III.6)-(III.7) and (B2)-(B3) we get

$$\chi_1 = -\left(|\mu_{23}|^2/k\,\varepsilon_0\right)\sum_k A_{1k}^{-1}\, S_1(k) \tag{B4}$$

$$\varkappa_1 = -\left(|\mu_{23}|^2/\hbar\,\varepsilon_0\right)\sum_k A_{1k}^{-1}\, S_{-1}^*(k) \tag{B5}$$

$$\chi_{-1} = -\left(|\mu_{23}|^2/\hbar\,\varepsilon_0\right)\sum_k (A_{4k}^{-1})^*\, S_{-1}(k) \tag{B6}$$

$$\varkappa_{-1} = -\left(|\mu_{23}|^2/\hbar\,\varepsilon_0\right)\sum_k \left(A_{4k}^{-1}\right)^* S_1^*(k) \tag{B7}$$

The general analytical formulas for $\chi_{\pm 1}$ and $\kappa_{\pm 1}$ are too complicated to be reproduced here. The self-terms $\chi_{\pm 1}$ depend only on the strong mode intensities $\alpha^2 (\equiv|\alpha|^2)$, $\beta_0{}^2$ and their detunings ; the coupling coefficients $\kappa_{\pm 1}$ have the functional shape $\beta_0\beta_0 f_{\pm 1}(\alpha^2, \beta^2, \Delta_{ij})$ where $f_{\pm 1}$ again depend only on the field intensities and detunings.

As an analytical example we study the weak pumping limit described by Eqs (A22)-(A24). For simplicity we solve the coupling terms only to the lowest non-vanishing order in β_0. From (A22) we see that besides the population beat term $D_{23}(1)$ also the quadrupole coherence ρ_{31} introduces mode couplings - this is an additional complication of the three-level system as compared to the two-level case of [7]. A straightforward solution of (A22)-(A24) gives to order $O(\alpha^2\beta_0{}^2)$

$$\begin{aligned}\rho_{23}(1) = \rho_{23}(1)_{SP} - \beta_{-1}^*\,\beta_0\,\beta_0\,\alpha^2 n_1^0\, i\, \mathcal{L}_{23}(1) \\ \Big\{\mathcal{L}_{21}^*(0)\,\mathcal{L}_{31}^*(0)\,\mathcal{L}_{21}^*(-1)\,\mathcal{L}_{31}^*(-1) \\ +\mathcal{L}_{21}^*(0)\,\mathcal{L}_{31}^*(0)\,\frac{\mathcal{L}_{21}^*(-1)+2\mathcal{L}_{23}(0)}{\Gamma - i\delta} \\ +\mathcal{L}_{21}(0)\,\mathcal{L}_{31}(1)\,\frac{\mathcal{L}_{21}(1)+2\mathcal{L}_{23}^*(-1)}{\Gamma - i\delta} \\ +4\,\frac{[\mathrm{Re}\,\mathcal{L}_{21}(0)][\mathcal{L}_{23}^*(-1)+\mathcal{L}_{23}(0)]}{\Gamma(\Gamma - i\delta)}\Big\}\end{aligned} \tag{B8}$$

where $\rho_{23}(1)_{SP}$ is the single-probe contribution. The expression for $\rho_{23}(-1)$ is obtainable from (B8) by an interchange of the indices 1 and -1 and by replacing δ by $-\delta$. The two-level case is found by letting the Lorentzian $\mathcal{L}_{31} \to 0$, so that just the last term in the braces in (B8) survives. As mentioned previously the coupling term depends on the relative phase via the factor $\beta_{-1}^{*}\beta_0\beta_0$. Resonances occuring in the cross coupling terms can be deduced from the Lorentzians in (B8).

According to (III.9)-(III.10) the two probe amplitudes $\beta_{\pm 1}$ evolve according to

$$\dot{\beta}_{-1} = g_{-1}\beta_{-1} + c_{-1}\beta_{1}^{*} \tag{B9}$$

$$\dot{\beta}_{1} = g_{1}\beta_{1} + c_{1}\beta_{-1}^{*} \tag{B10}$$

where

$$g_{\pm 1} = -\frac{\nu_0}{2Q} - i\left(\nu_{c,\pm 1} - \nu_{\pm 1}\right) + \frac{1}{2} i \nu_0 \chi_{\pm 1} \tag{B11}$$

$$c_{\pm 1} = \frac{1}{2} i \nu_0 \varkappa_{\pm 1} \tag{B12}$$

Using Laplace transforms, we get with the initial values $\{\beta_1(0), \beta_{-1}(0)\}$

$$\beta_1(s) = [(s - g_{-1}^{*})\beta_1(0) + c_1\beta_{-1}^{*}(0)] / D(s) \tag{B13}$$

$$\beta_{-1}^{*}(s) = [(s - g_1)\beta_{-1}^{*}(0) + c_{-1}^{*}\beta_1(0)] / D(s) \tag{B14}$$

where

$$D(S) = (S-g_1)(S-g_{-1}^*) - c_1 c_{-1}^* \qquad \text{(B15)}$$

The characteristic roots, $D(S_{1,2}) = 0$, determine the temporal evolution of the system. Note that the sign of $\mathrm{Im}(S_{1,2})$ depends on the choice of the combination $\{\beta_1, \beta_{-1}^*\}$ - in the case $\{\beta_1^*, \beta_{-1}\}$ we would have obtained the characteristic equation $D^*(S) = 0$. When fixing the sign of the square root of the complex expression in either (III.11) or when solving $S_{1,2}$ from (B15) one must use the branches which reproduce the correct roots in the limit $C_{\pm 1} \rightarrow 0$, i.e. $S_1 \rightarrow g_1$ and $S_2 \rightarrow g_{-1}^*$.

Inversion of (B13)-(B14) yields

$$\beta_1(t) = \{[(S_1 - g_{-1}^*)\beta_1(0) + c_1\beta_{-1}^*(0)]e^{S_1 t} - [(S_2 - g_{-1}^*)\beta_1(0) + c_1\beta_{-1}^*(0)]e^{S_2 t}\}/(S_1 - S_2) \qquad \text{(B16)}$$

$$\beta_{-1}^*(t) = \{[(S_1 - g_1)\beta_{-1}^*(0) + c_{-1}^*\beta_1(0)]e^{S_1 t} - [(S_2 - g_1)\beta_{-1}^*(0) + c_{-1}^*\beta_1(0)]e^{S_2 t}\}/(S_1 - S_2) \qquad \text{(B17)}$$

With the particular initial values

$$\beta_1(0)/\beta_{-1}^*(0) = -c_1/(S_2 - g_{-1}^*) \qquad \text{(B18)}$$

both $\beta_1(t)$ and $\beta^*_{-1}(t)$ evolve as $\exp(S_1 t)$ and their amplitude ratio remains at the constant value of (B18) - only one eigenmode of the system is excited. With the choice

$$\beta_1(0)/\beta^*_{-1}(0) = -c_1/(S_1 - g^*_{-1}) \tag{B19}$$

the second eigenmode corresponding to S_2 would be excited. For an arbitrary set $\{\beta_1(0),\beta^*_{-1}(0)\}$ both eigenmodes are present in the proportions given by (B16)-(B17).

The apparent evolution of the probe will depend on the inital values in addition to their growth rates. For instance, for $\beta_{-1}(0) = 0$ we get

$$\beta_1(t) = \beta_1(0)\left\{e^{S_1 t} + \frac{S_2 - g^*_{-1}}{S_1 - S_2}\left(e^{S_1 t} - e^{S_2 t}\right)\right\} \tag{B20}$$

$$\beta^*_{-1}(t) = \beta_1(0)\, c^*_{-1}\left(e^{S_1 t} - e^{S_2 t}\right)/(S_1 - S_2) \tag{B21}$$

For a weak coupling $|c^*_{-1}|$ and $|S_2 - g^*_{-1}|$ are both small implying that the dominant term is $\beta_1(0)\exp S_1 t$ provided that Re S_1>Re S_2. If Re S_2>Re S_1 the initial single probe character will change to a bichromatic one after a few exponentiation periods 1/Re S_2. The initial behavior has to be kept in mind when using the gain curves for bichromatic modes in section III.

FIGURE CAPTIONS

Fig. 1 The three-level system considered. The pump α and the main FIR mode β_0 may be arbitrarily intense. The probe fields β_1 (with a frequency $\nu_1=\nu_0+\delta$) and $\beta_{-1}(\nu_{-1}=\nu_0-\delta)$ are assumed weak; ν_0 is the frequency of β_0.

Fig. 2 Typical single mode gain spectra for a resonant pump ($\Delta_{21}=0$, $\alpha=5\gamma$) and $\beta_0/\gamma=1$, 2, 5 and 10 for curves 1 to 4. The plotted quantity is $\mathrm{Im}(\rho_{23}(0)/n_1{}^0)$ which is proportional to the instantaneous growth rate $|\dot{\beta}_0|\sim G(\beta_0)|\beta_0|$.

Fig. 3 As Fig. 2 but with a detuned pump ($\Delta_{21}=5\gamma$, $\alpha=5\gamma$). The Raman resonance at $\Delta_{23}=\Delta_{21}$ and the line center at $\Delta_{23}=0$ are shifted and get heavily distorted at high intensities.

Fig. 4 Single probe gain $\mathrm{Im}(\gamma\rho_{23}(1)/n_1{}^0\beta_1)$ for a detuned pump ($\Delta_{21}/\gamma=-4$ and $\alpha/\gamma=0.1$) with the main FIR mode at Raman resonance i.e. $\Delta_{23}/\gamma=-4$. The amplitude values β_0/γ are 0.1, 0.5, 0.75, 1., 1.5, 2., 3., 5. for the curves 1 to 8. The abscissa is the distance of the probe from the main mode in units γ, hence -4 is the line center position and 0 the Raman resonance.

Fig. 5 Growth rates $\mathrm{Re}(\lambda\pm)$ for a bichromatic probe (the intense field parameters are as in Fig. 4). We have chosen ν_1 to match Fig. 4. Since the probe component ν_{-1} is symmetric with ν_1 with respect to the position of the main mode, the gain curves are also fully symmetric. The actual field pattern must be calculated as outlined in Appendix B.

Fig. 6 As Fig. 5 but with a strong pump : $\alpha/\gamma=3$

Fig. 7 Single probe gain for a resonant pump ($\alpha/\gamma=0.1$) and a resonant main FIR mode. Curve parameters : $\beta_0/\gamma=0.1$, 0.5, 0.75, 1, 1.5, 2, 3, 5 (as in Fig. 4) for curves 1 to 8; $\beta_1=0.1\gamma$.

Fig. 8 As in Fig. 7 but with an intense pump, $\alpha/\gamma=3$.

Fig. 9 Growth rates for a bichromatic probe corresponding to the parameters of Fig. 7.

Fig.10 As Fig. 9 but with an intense pump $\alpha/\gamma=3$.

Fig.11 Representative resonance structure of the single probe gain under intense field conditions. In Fig. 11a we have parameters $\Delta_{21}=0$, $\Delta_{23}/\gamma=10$, $\alpha/\gamma=11$, $\beta_0/\gamma=7$ and $\beta_1/\gamma=0.1$. The top part shows the gain and the bottom part the dispersion. The broken lines denote resonance positions predicted by the dressed atom model. In Fig. 11b (dispersion omitted) we have $\Delta_{21}=\Delta_{23}=10\gamma$ and the rest of the parameters as in Fig. 11a. In Fig. 11c, $\Delta_{21}=\Delta_{23}=0$, $\alpha/\gamma=8$ and $\beta_0/\gamma=5$.

Fig.12 Contour plots of the single mode probe gain on the $(\beta_0, \omega_{23}-\nu_1)$ plane for $\Delta_{21}=\Delta_{23}=0$ and $\alpha=3\gamma$. The $\pm$ signs indicate regions of gain and absorption. The curves are shown in steps of 2.4×10^{-3}.

The broken lines indicate the resonances predicted by the dressed atom model.

Fig.13 As Fig.12 but for $\Delta_{21}=\Delta_{23}=10\gamma$. Step = 10^{-3}.

Fig.14 As Fig. 13 but with an increased value of $\alpha/\gamma=10$. The hatched region displays stable single mode operation for the case of cavity losses $C/Q=0.02$. (cf. Eq. (IV.1)).

Fig 1

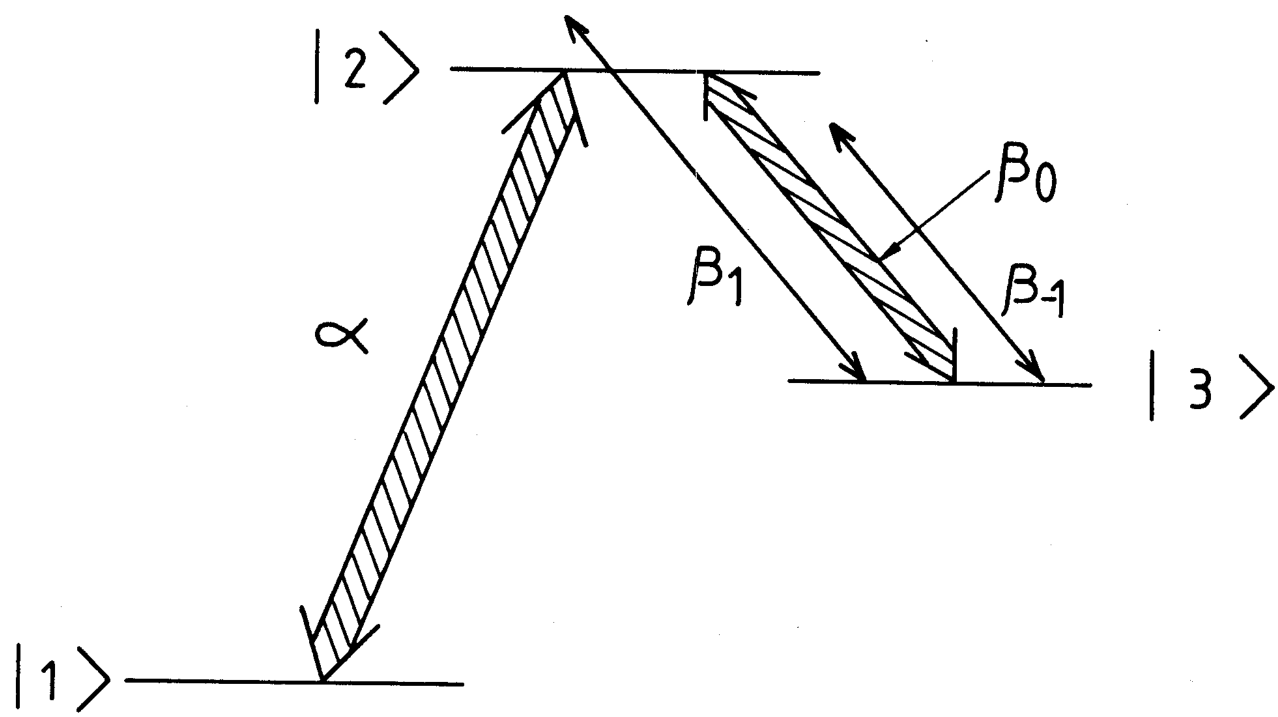

Fig 2

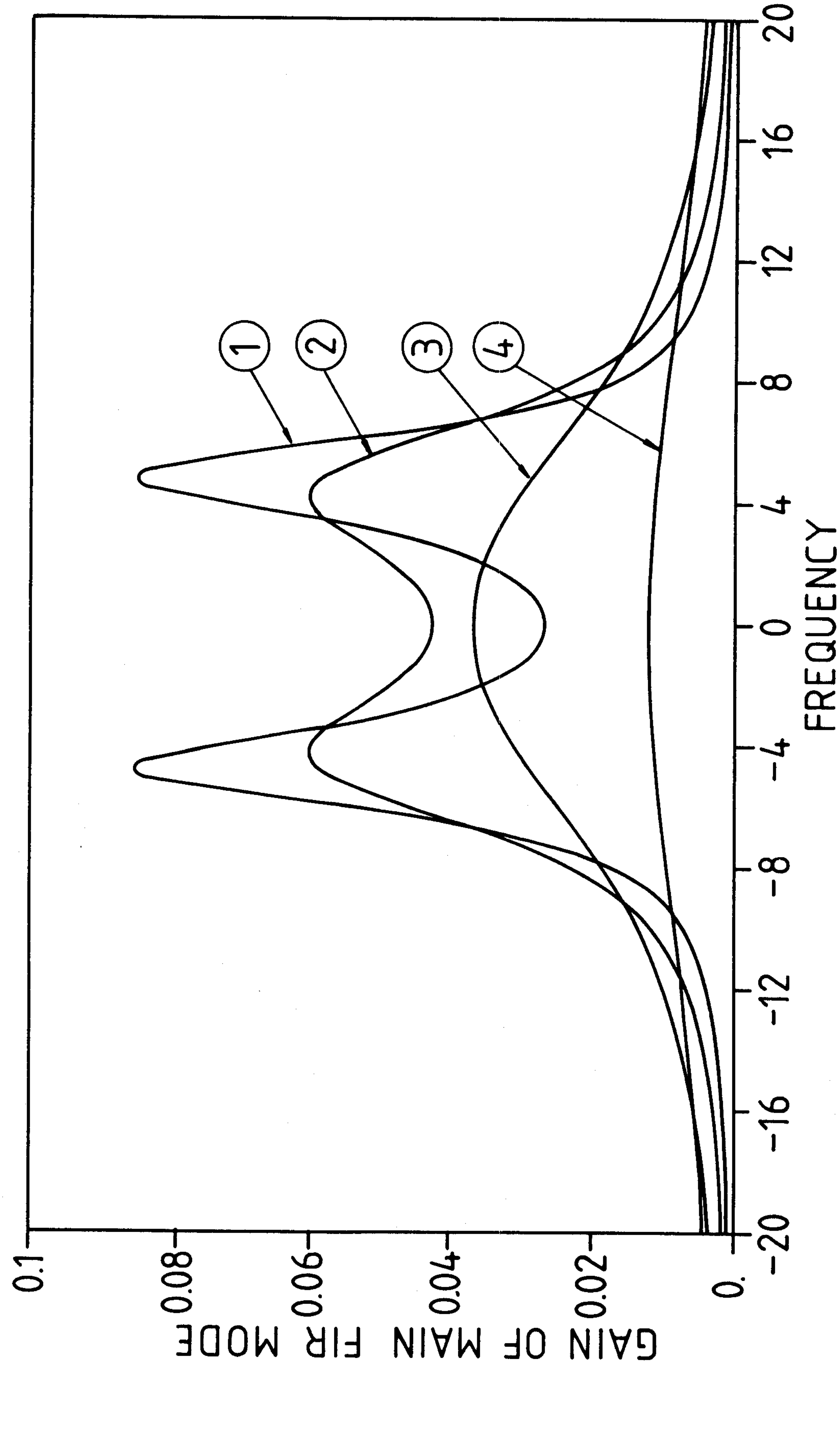
GAIN OF MAIN FIR MODE
0.1
0.08
0.06
0.04
0.02
0.
FREQUENCY
-20
-16
-12
-8
-4
0
4
8
12
16
20
1
2
3
4

Fig 3

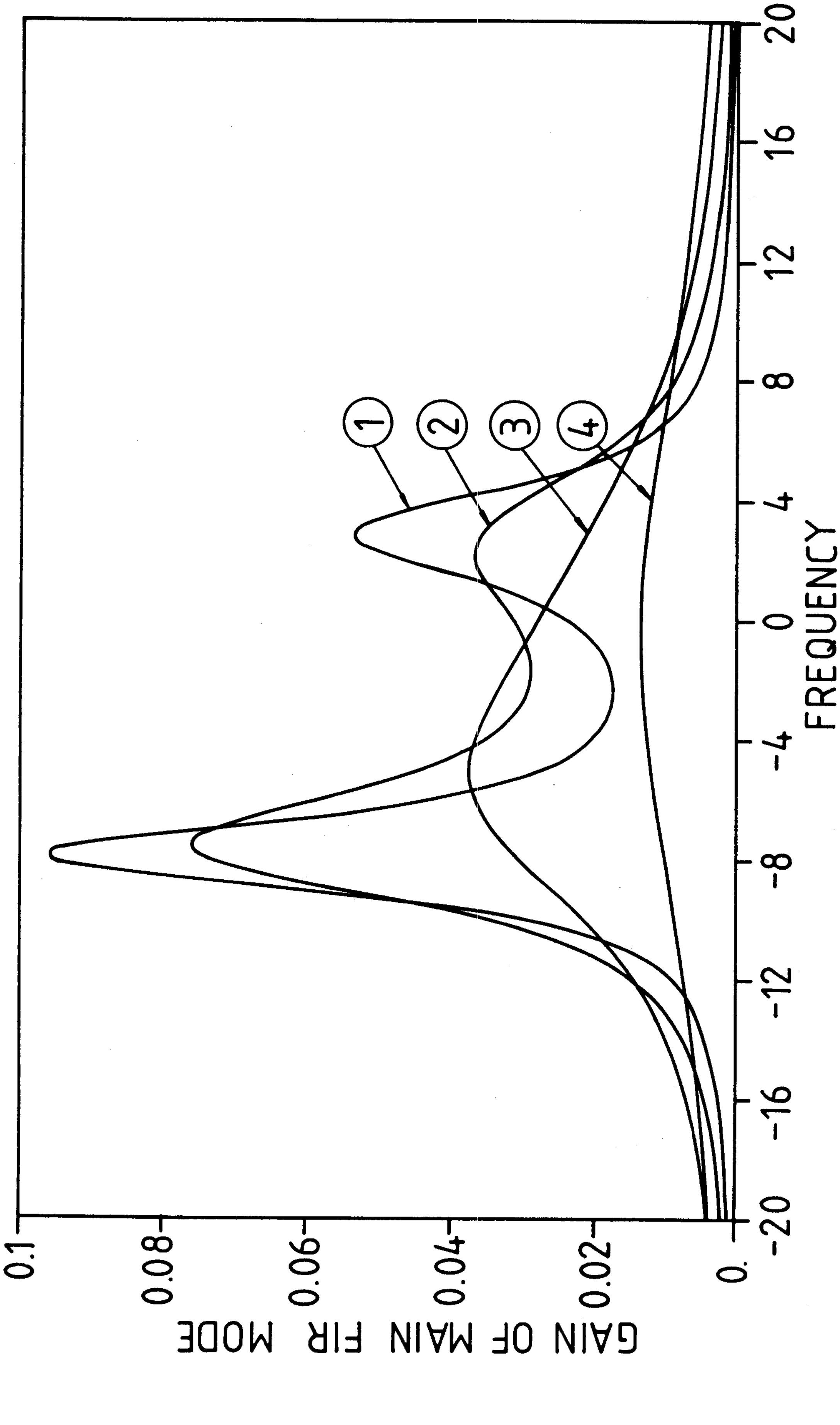

GAIN OF MAIN FIR MODE
0.
0.02
0.04
0.06
0.08
0.1
FREQUENCY
-20
-16
-12
-8
-4
0
4
8
12
16
20
1
2
3
4

Fig 4

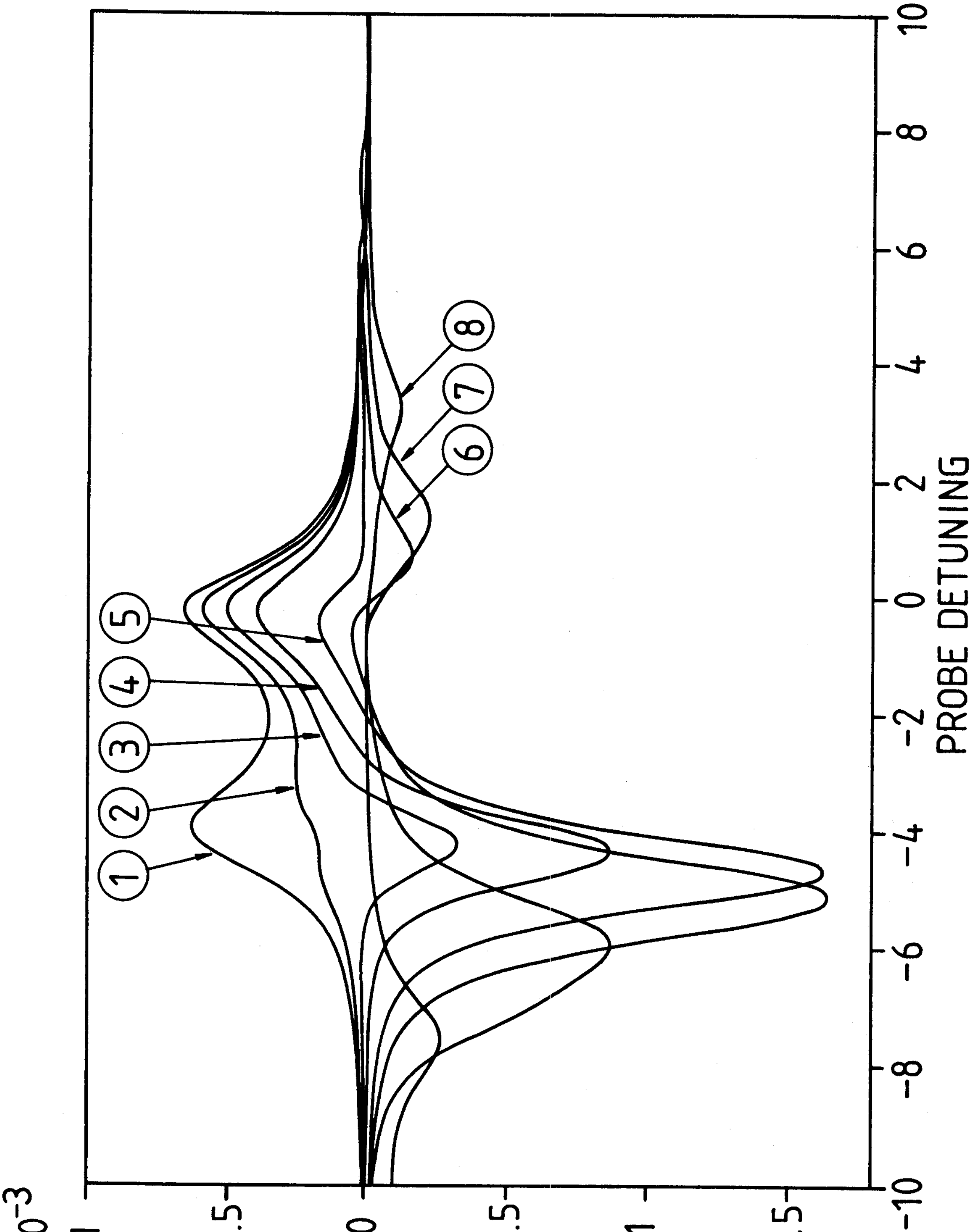

PROBE GAIN
*10^-3
1
0.5
0
-0.5
-1
-1.5
PROBE DETUNING
-10
-8
-6
-4
-2
0
2
4
6
8
10
1
2
3
4
5
6
7
8

Fig 5a

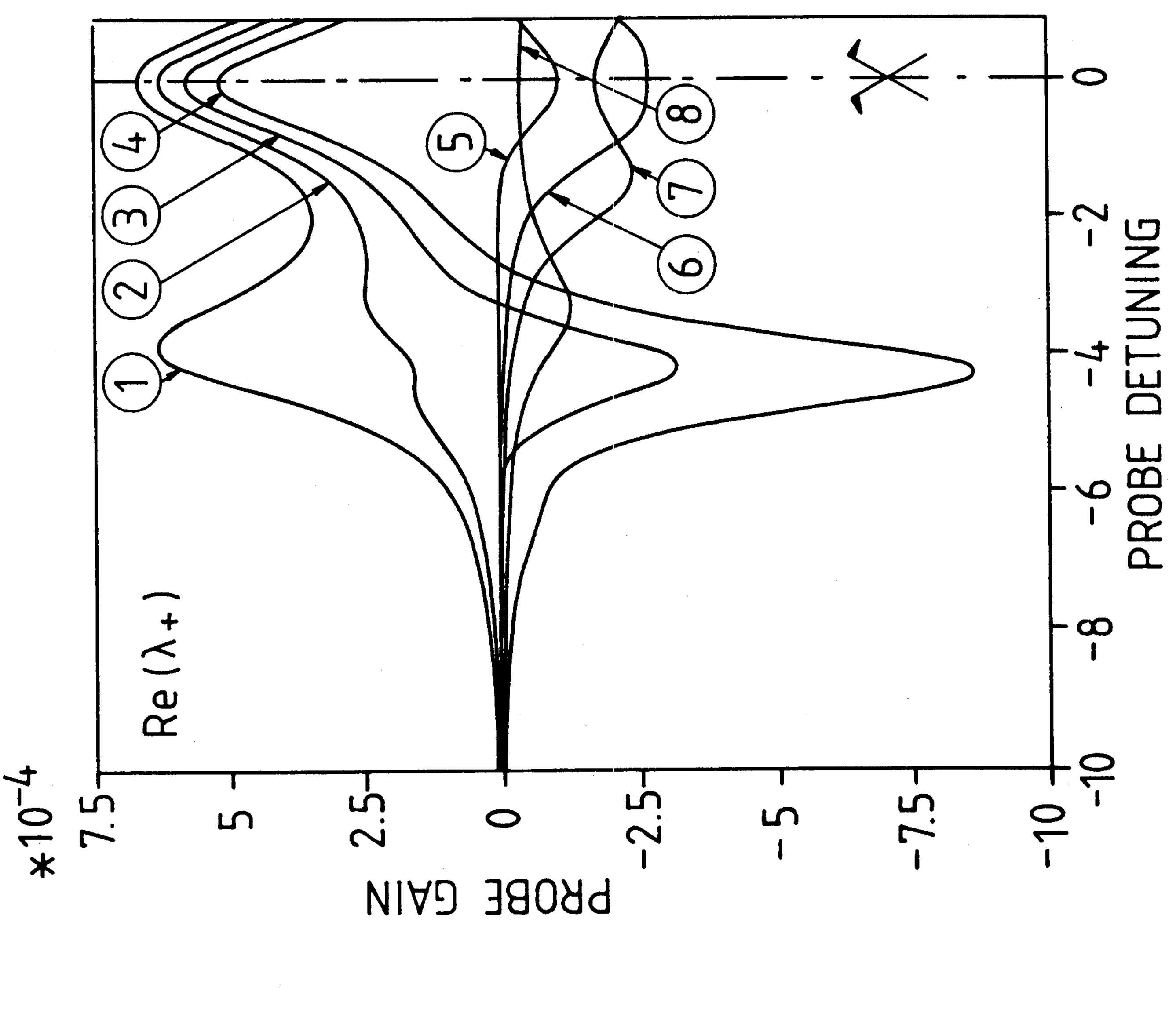
PROBE GAIN
*10^-4
7.5
5
2.5
0
-2.5
-5
-7.5
-10
-10
-8
-6
-4
-2
0
PROBE DETUNING
Re(λ+)
1
2
3
4
5
6
7
8

Fig. 5b

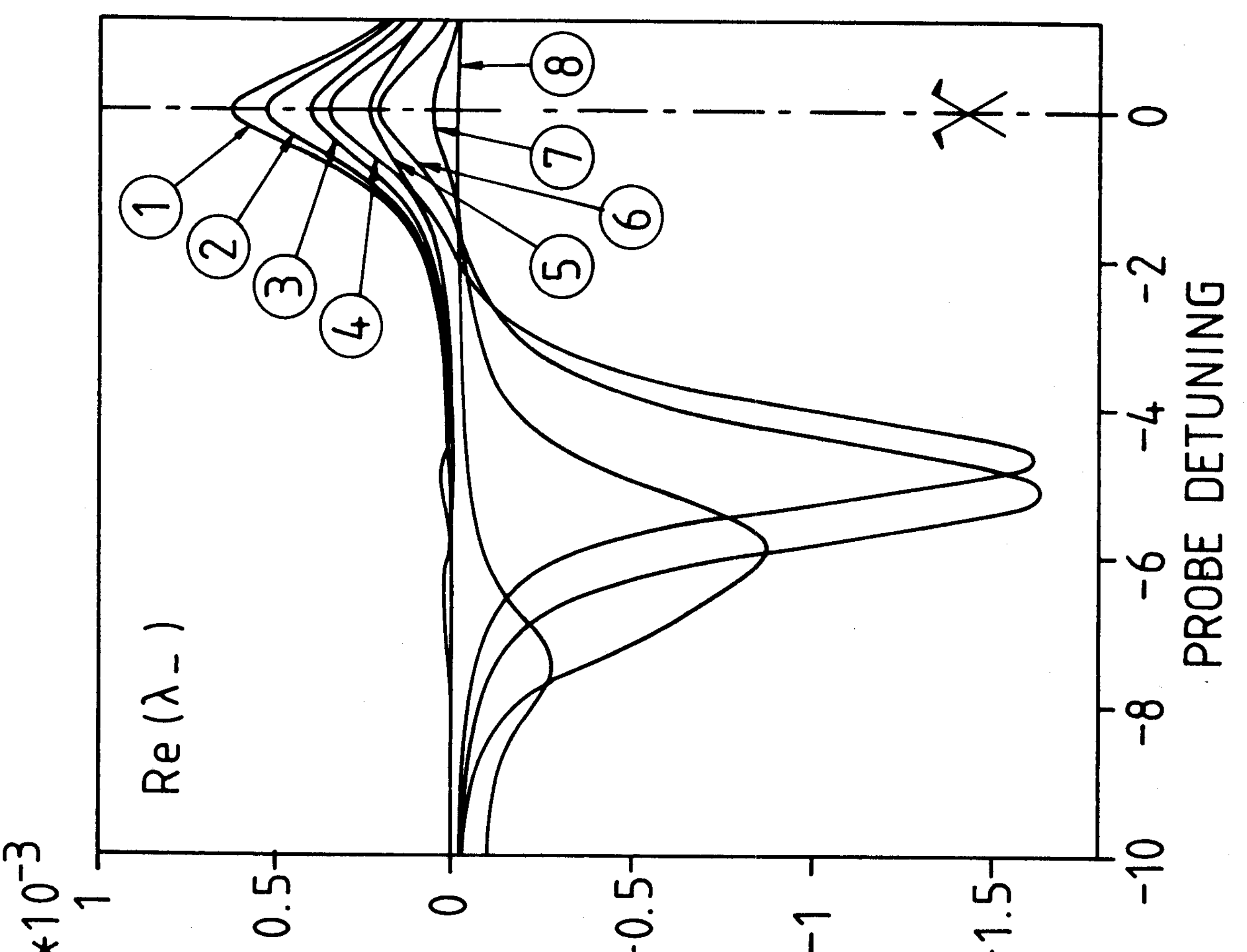

*10^-3
PROBE GAIN
1
0.5
0
-0.5
-1
-1.5
Re (λ_)
-10
-8
-6
-4
-2
0
PROBE DETUNING
1
2
3
4
5
6
7
8

Fig 6a

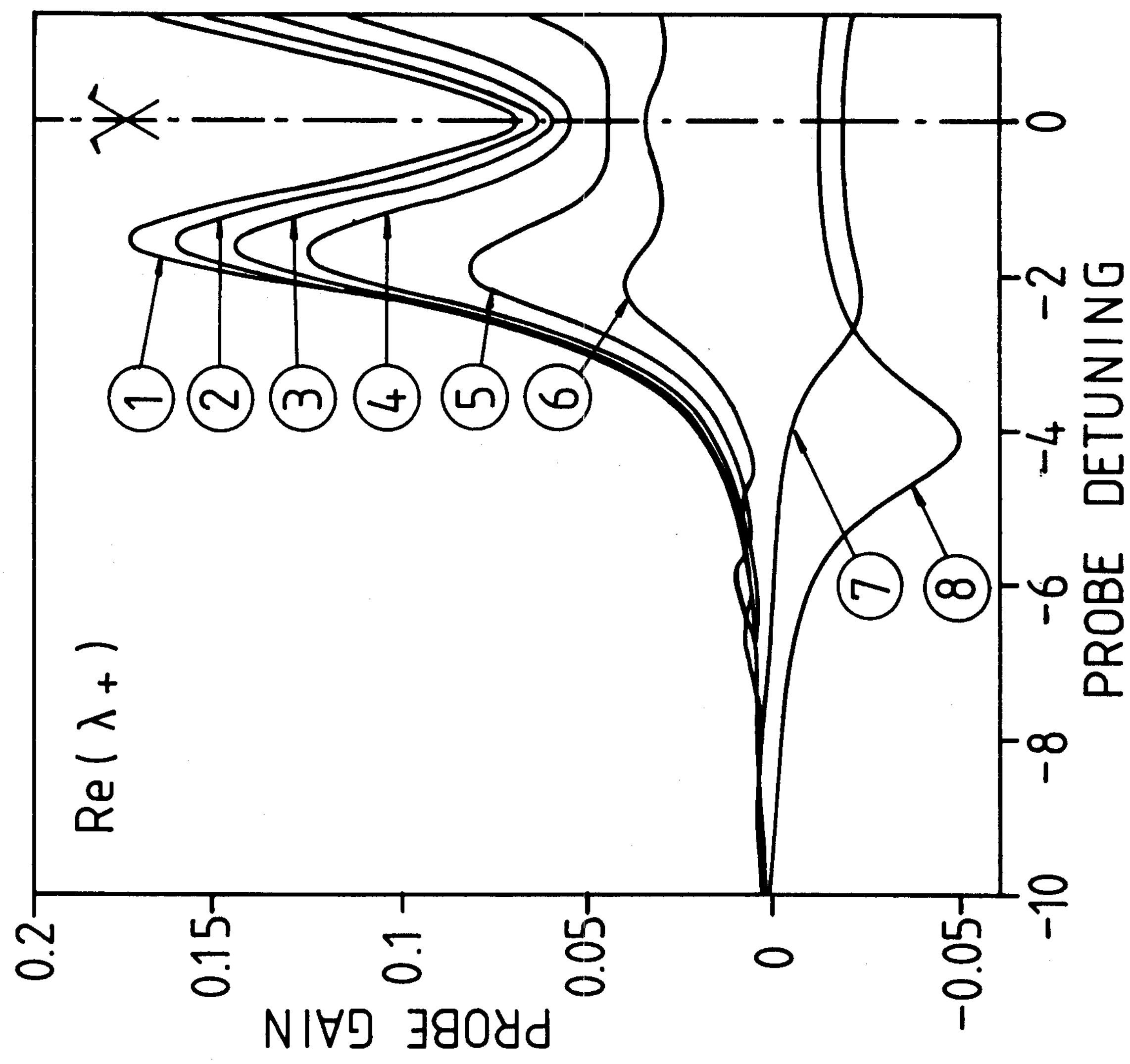

Re (λ +)
PROBE GAIN
0.2
0.15
0.1
0.05
0
−0.05
PROBE DETUNING
−10
−8
−6
−4
−2
0
1
2
3
4
5
6
7
8

Fig 6b

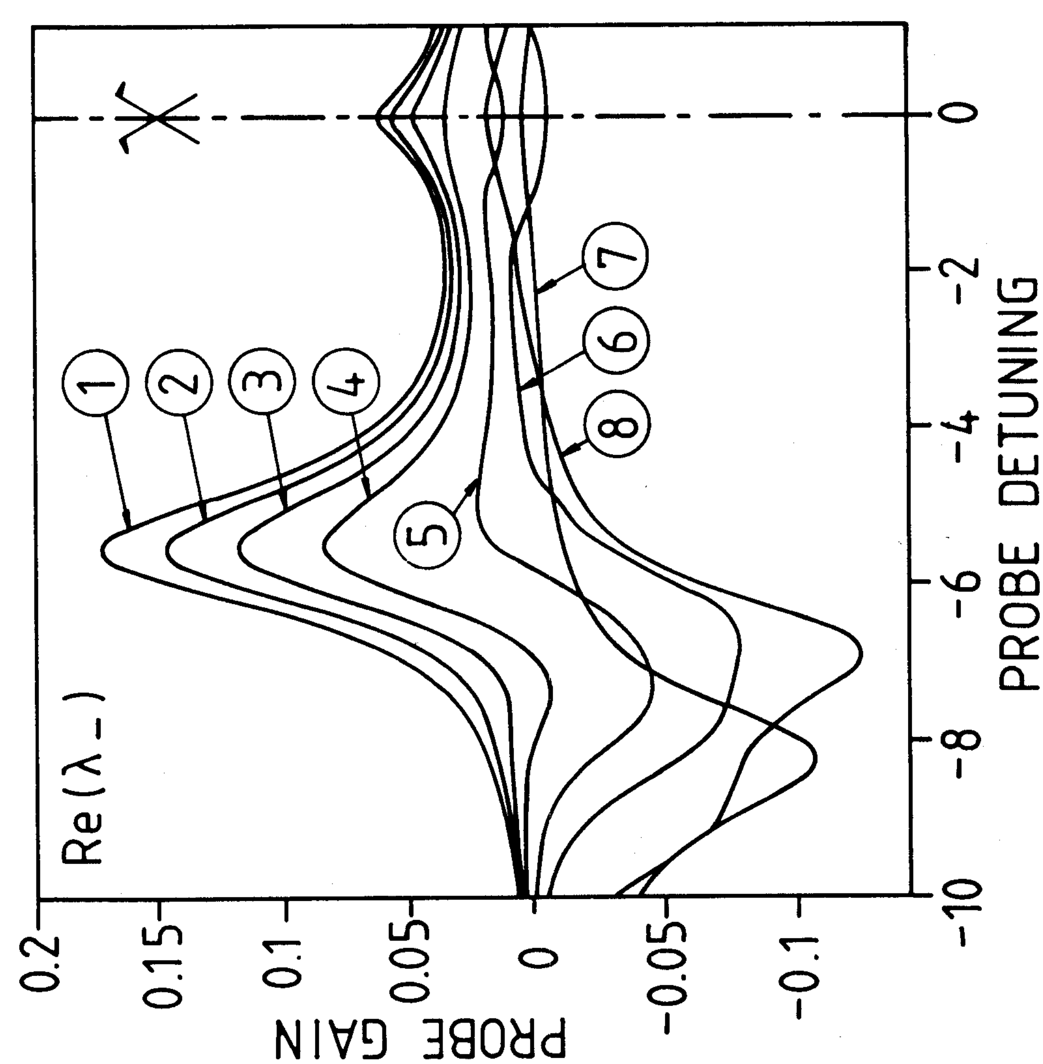

Re(λ_)
PROBE GAIN
PROBE DETUNING
0.2
0.15
0.1
0.05
0
-0.05
-0.1
-10
-8
-6
-4
-2
0
1
2
3
4
5
6
7
8

Fig 7

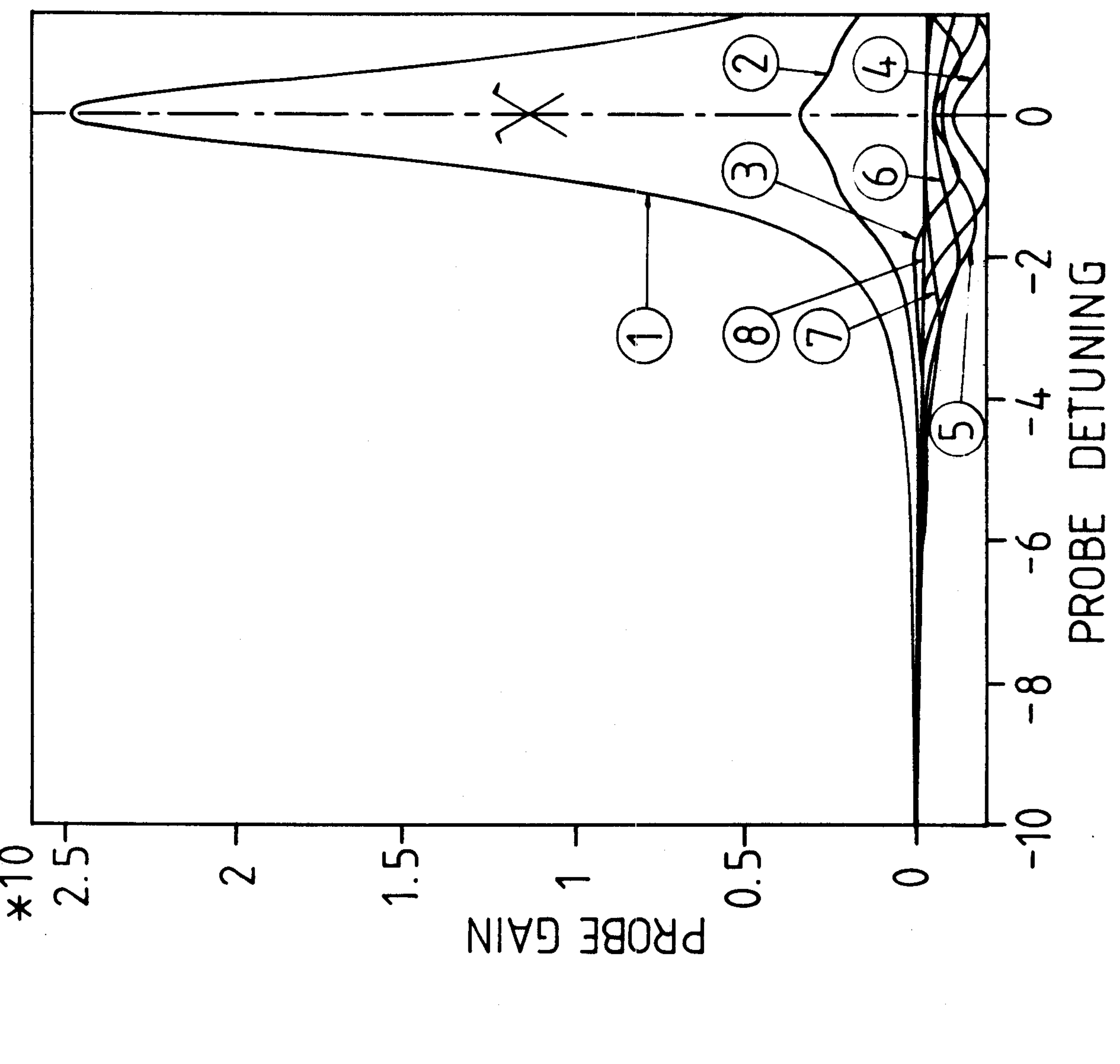

Fig 8

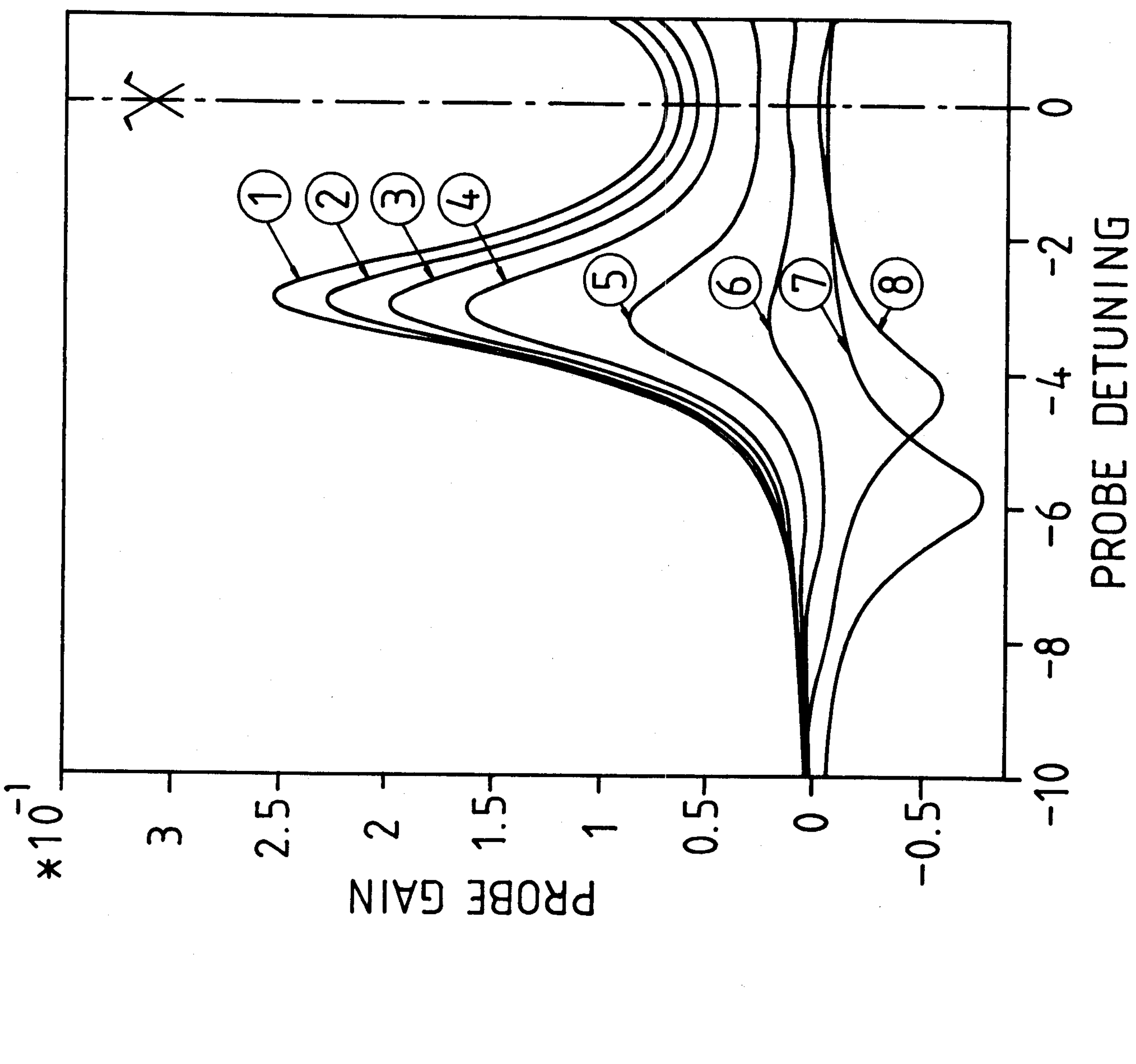

*10^-1
PROBE GAIN
3
2.5
2
1.5
1
0.5
0
-0.5
-10
-8
-6
-4
-2
0
PROBE DETUNING
1
2
3
4
5
6
7
8

Fig 9a

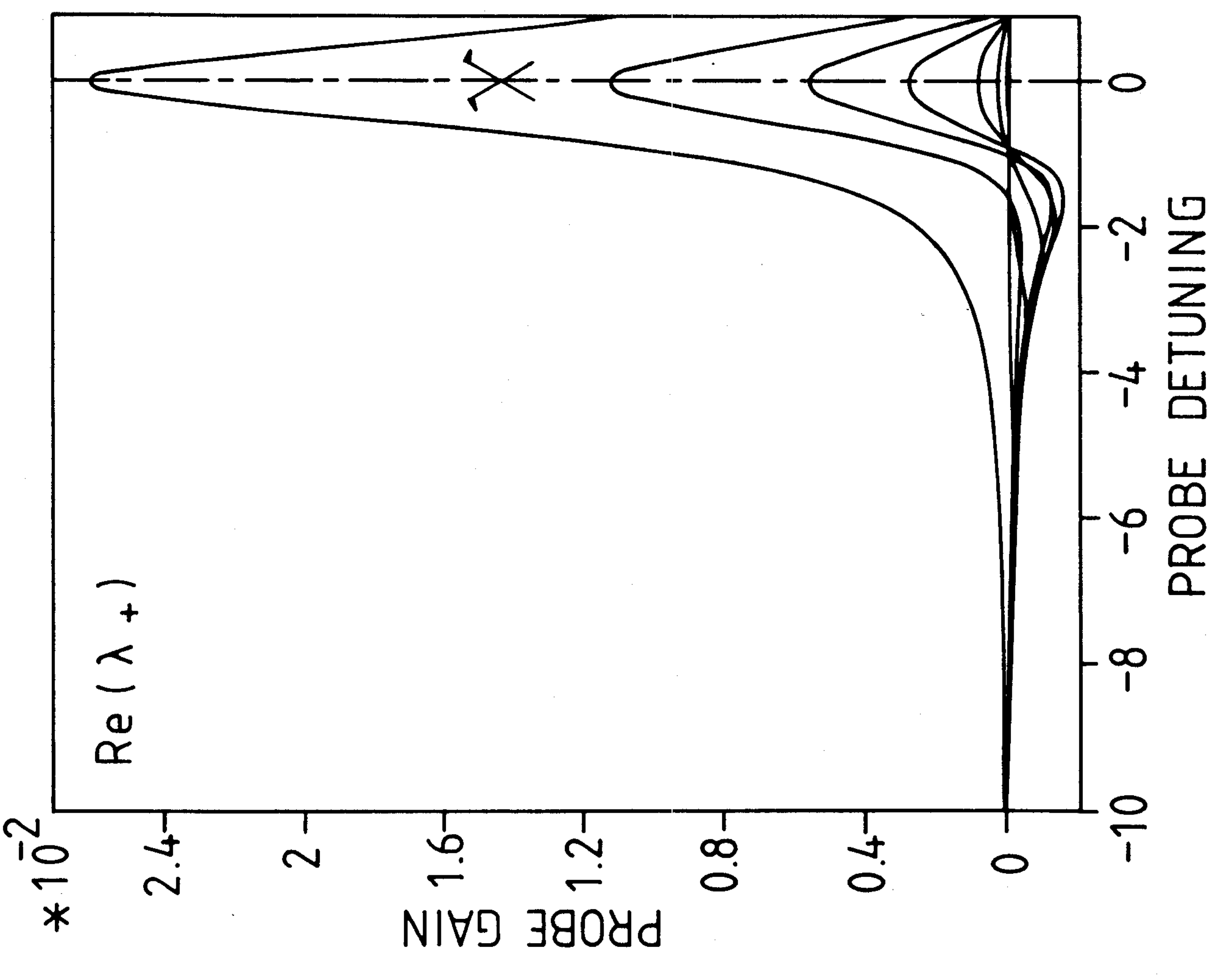

Fig 9b

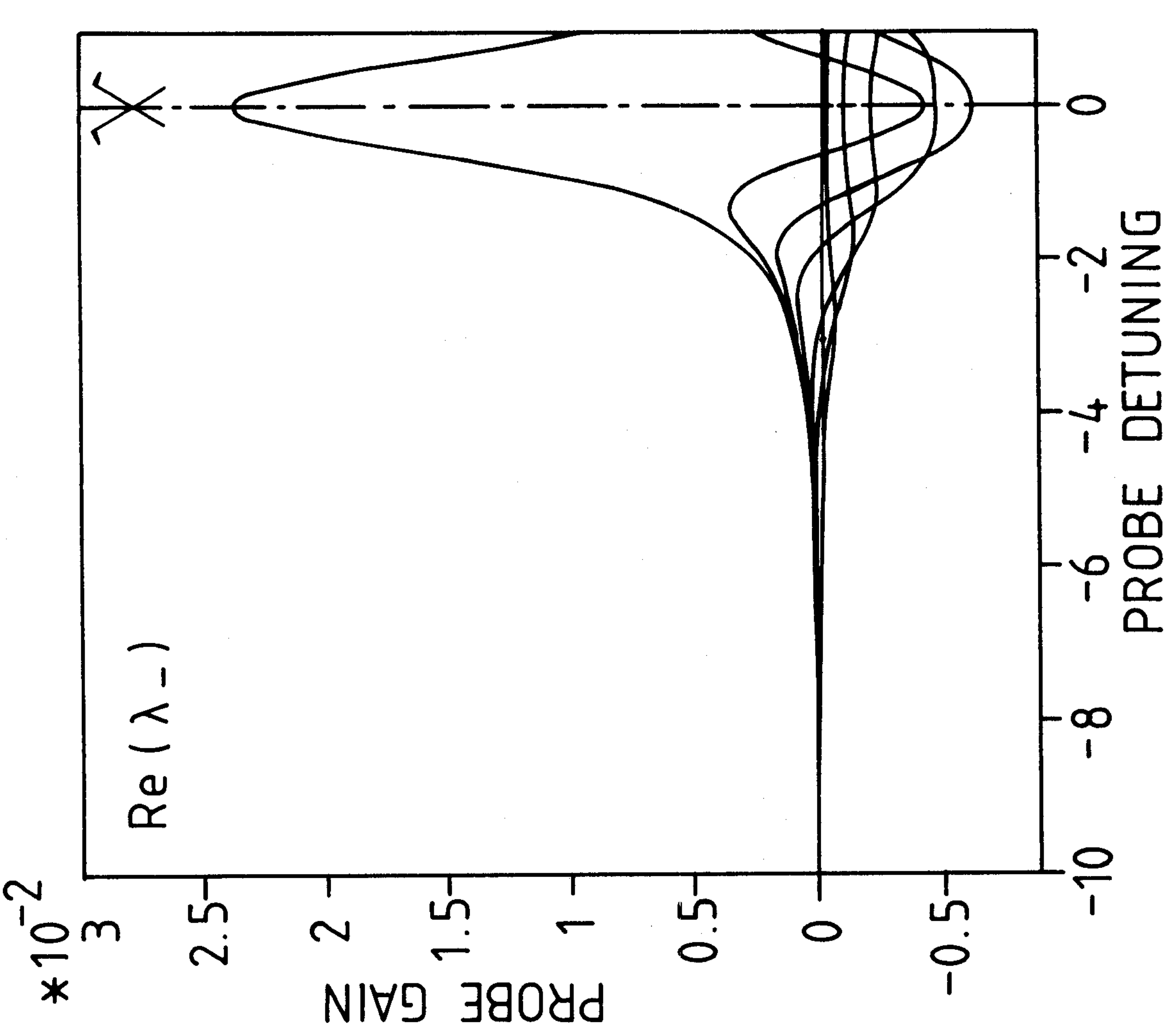

Fig 10a

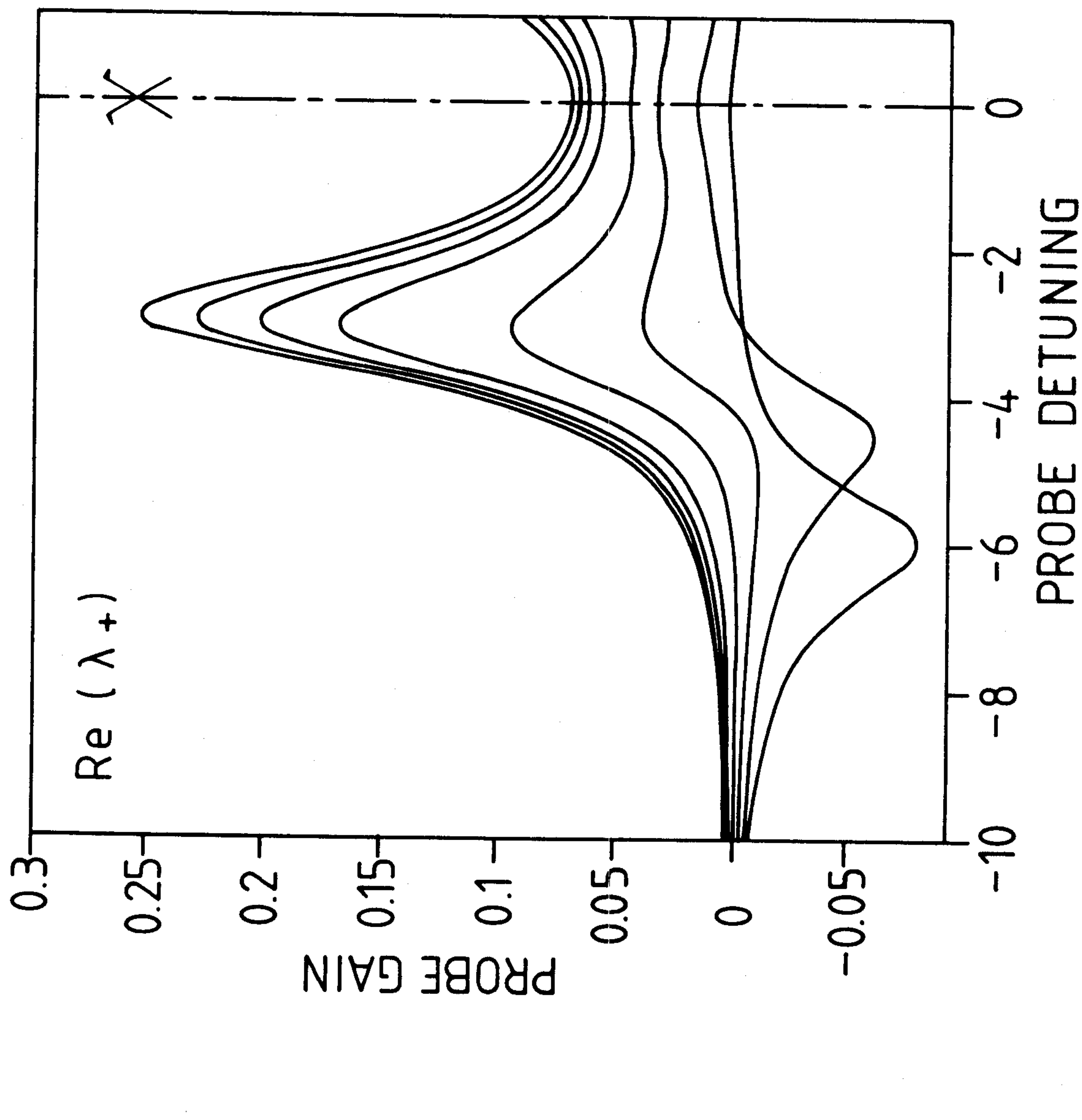
Re (λ +)
PROBE GAIN
0.3
0.25
0.2
0.15
0.1
0.05
0
−0.05
PROBE DETUNING
−10
−8
−6
−4
−2
0

Fig 10b

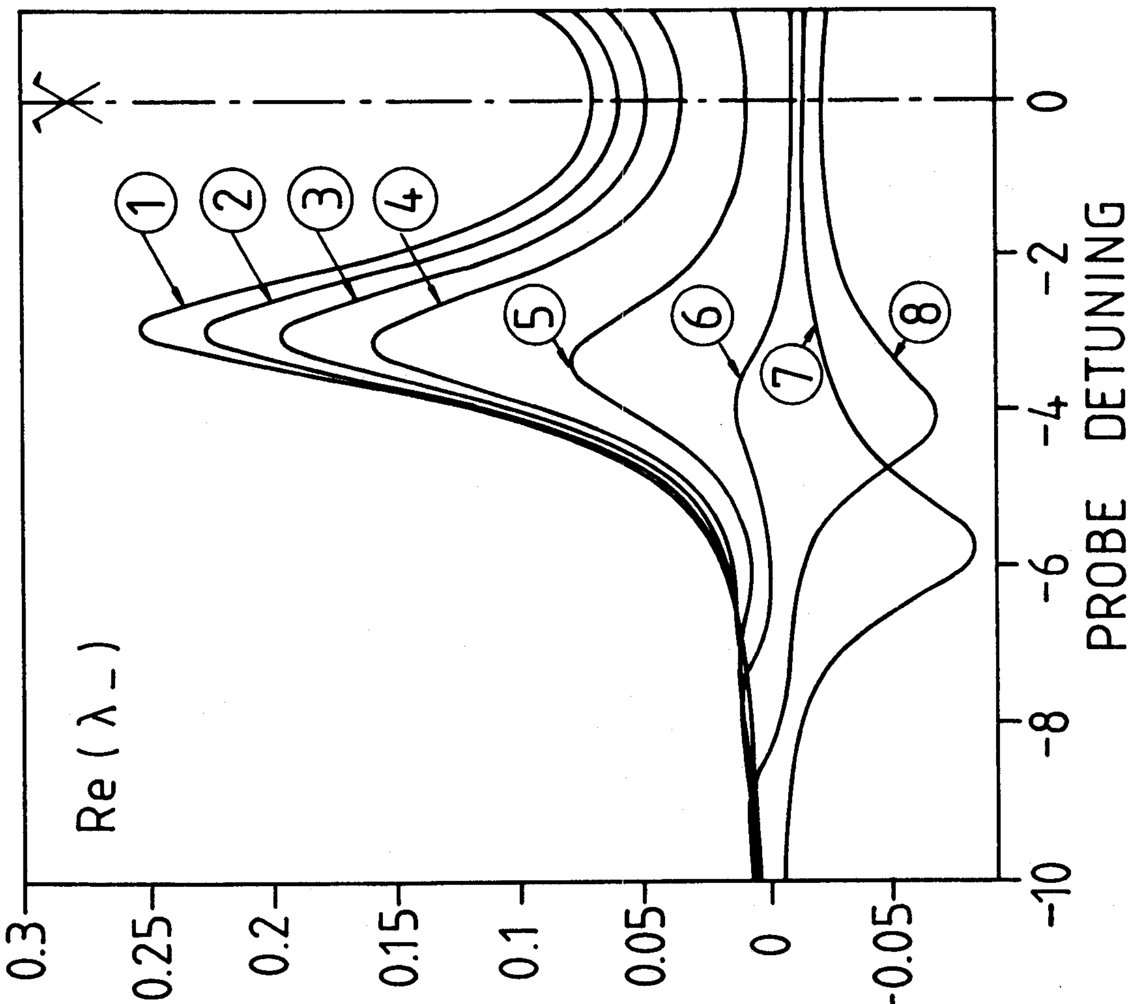

Re (λ_)
PROBE GAIN
PROBE DETUNING
0.3
0.25
0.2
0.15
0.1
0.05
0
−0.05
−10
−8
−6
−4
−2
0
1
2
3
4
5
6
7
8

Fig 11a
lower part

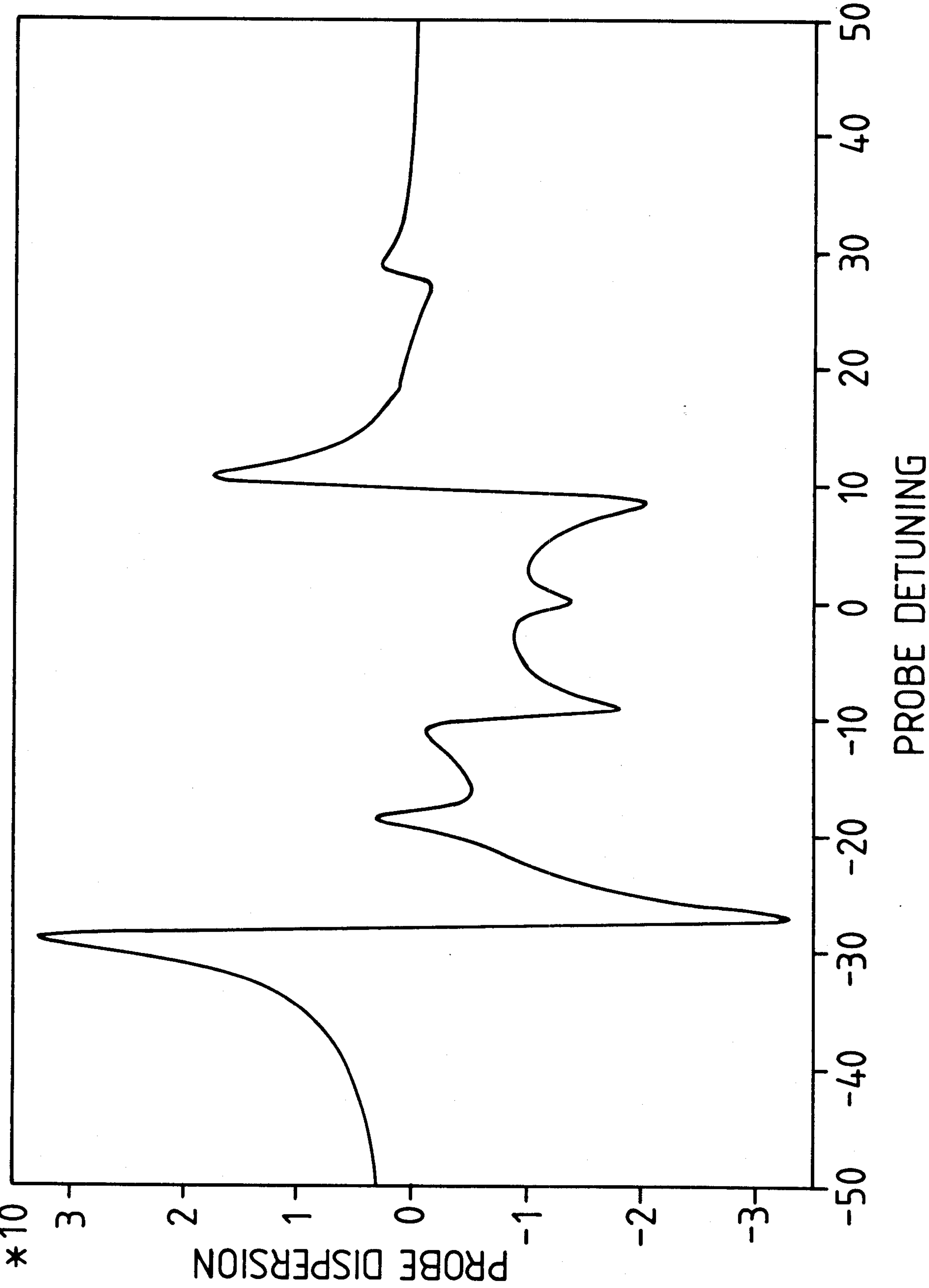

Fig 11 a upper part

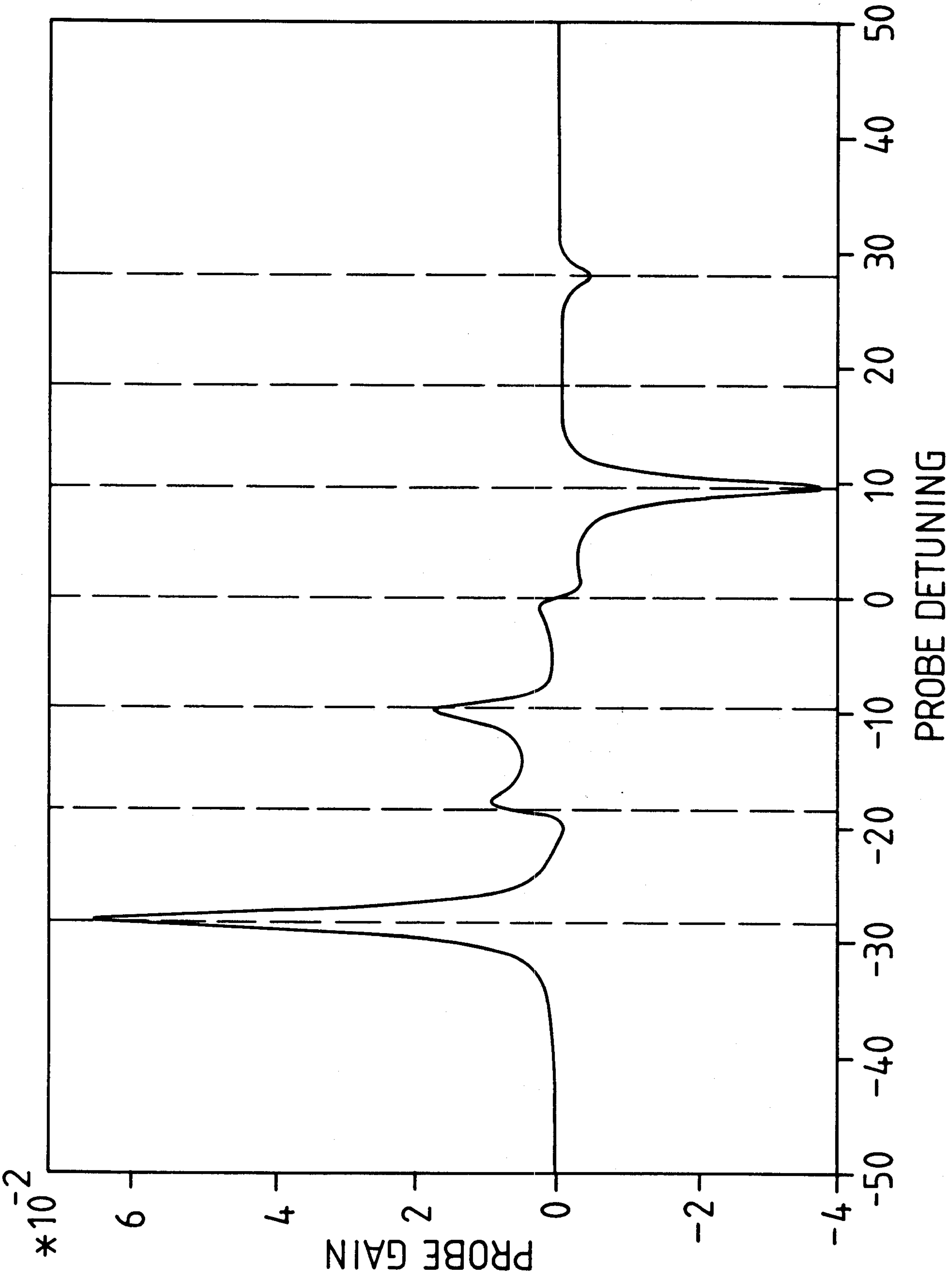

Fig 11a
lower part

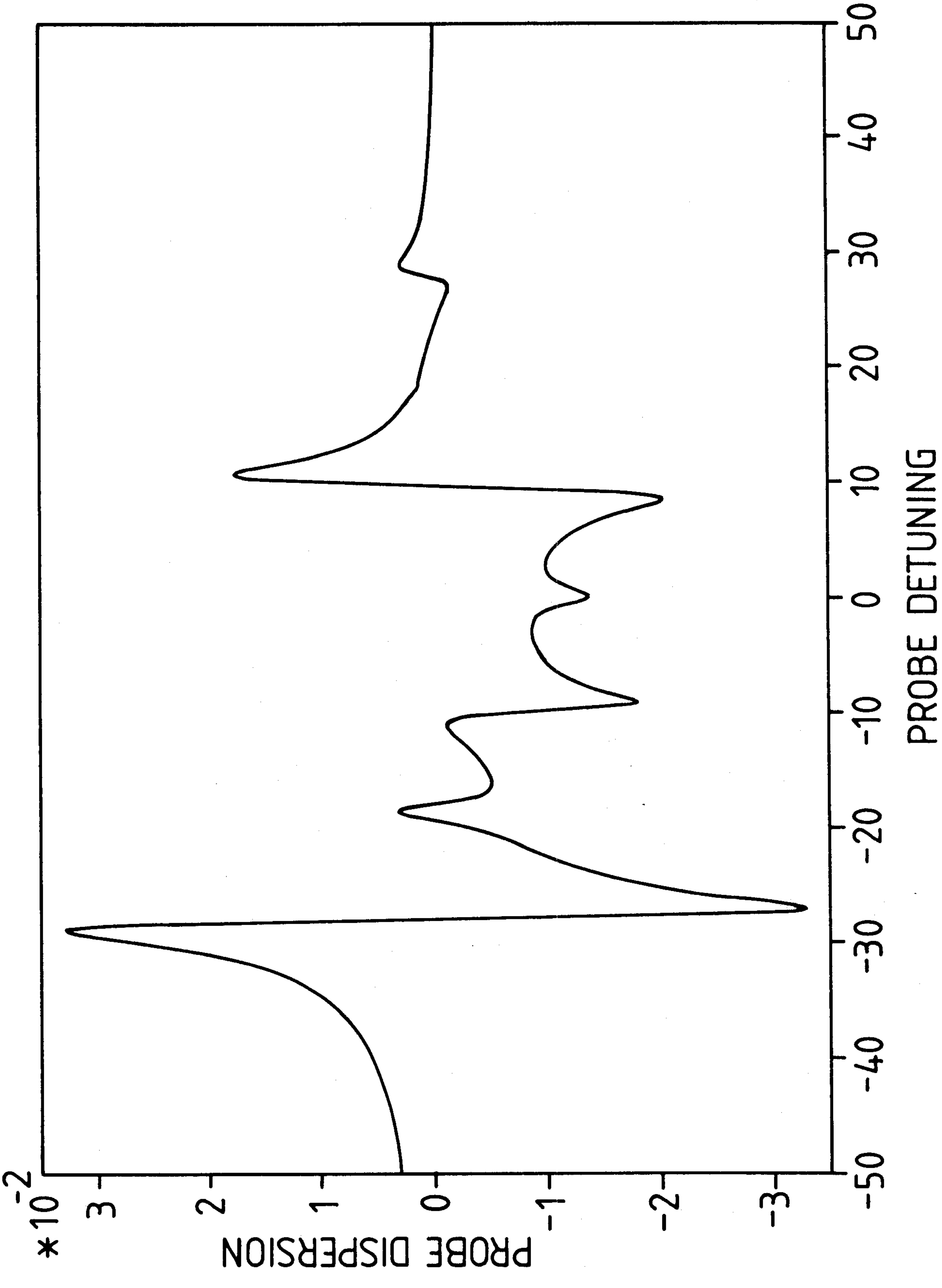

Fig 11b

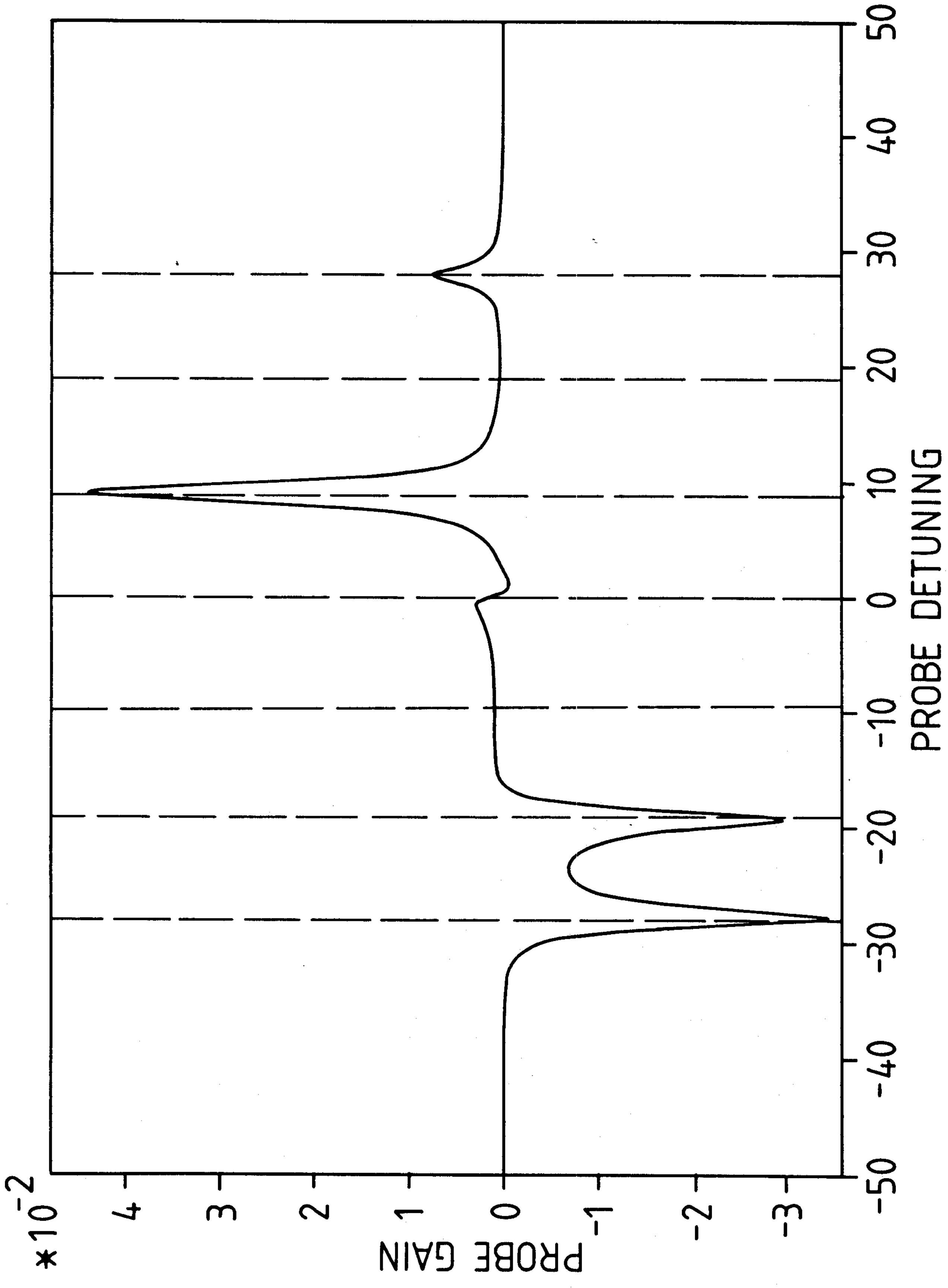

PROBE GAIN
*10^-2
4
3
2
1
0
-1
-2
-3
PROBE DETUNING
-50
-40
-30
-20
-10
0
10
20
30
40
50

Fig 11c

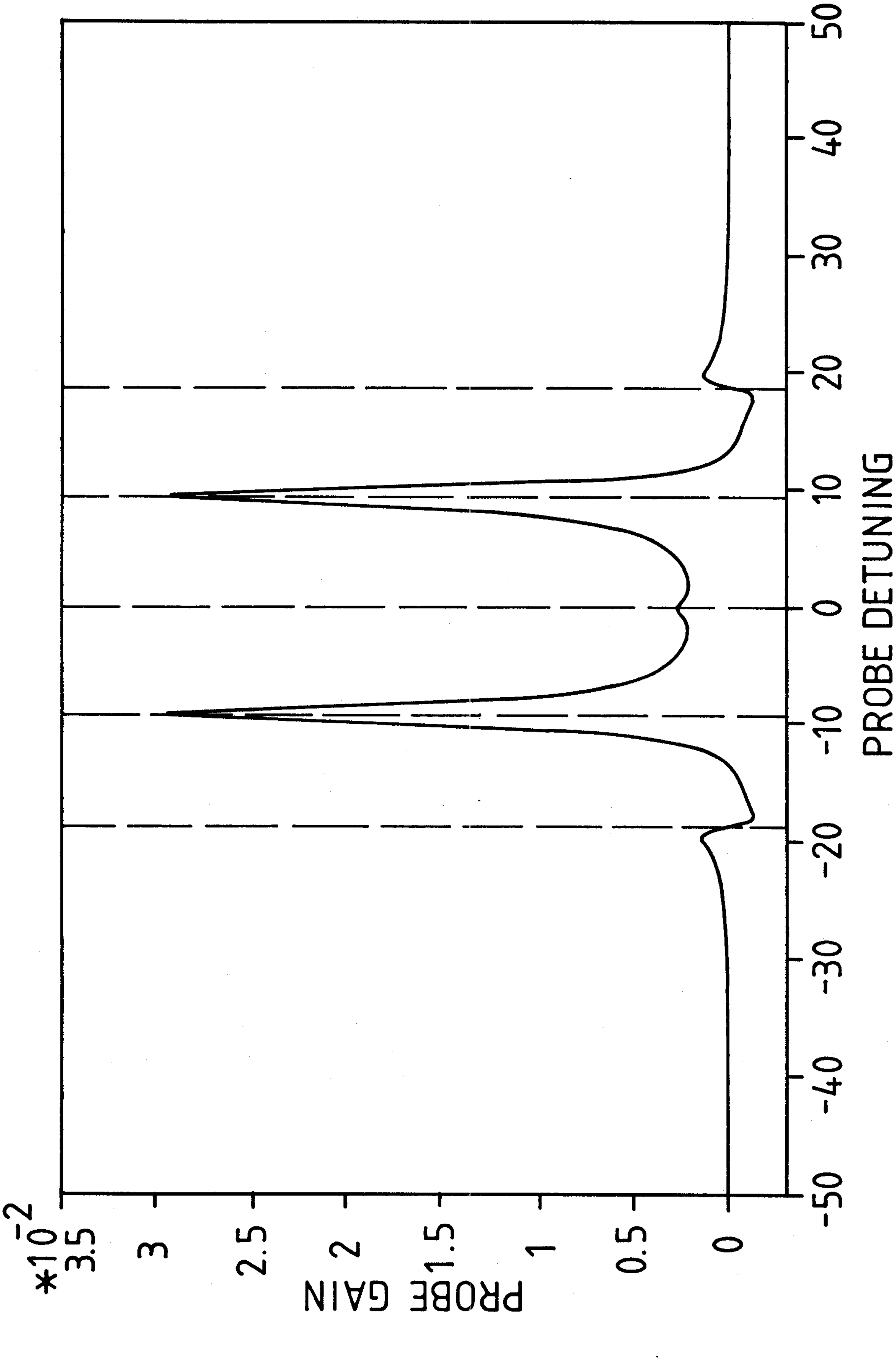
PROBE GAIN
*10^-2
0
0.5
1
1.5
2
2.5
3
3.5
PROBE DETUNING
-50
-40
-30
-20
-10
0
10
20
30
40
50

Fig 12

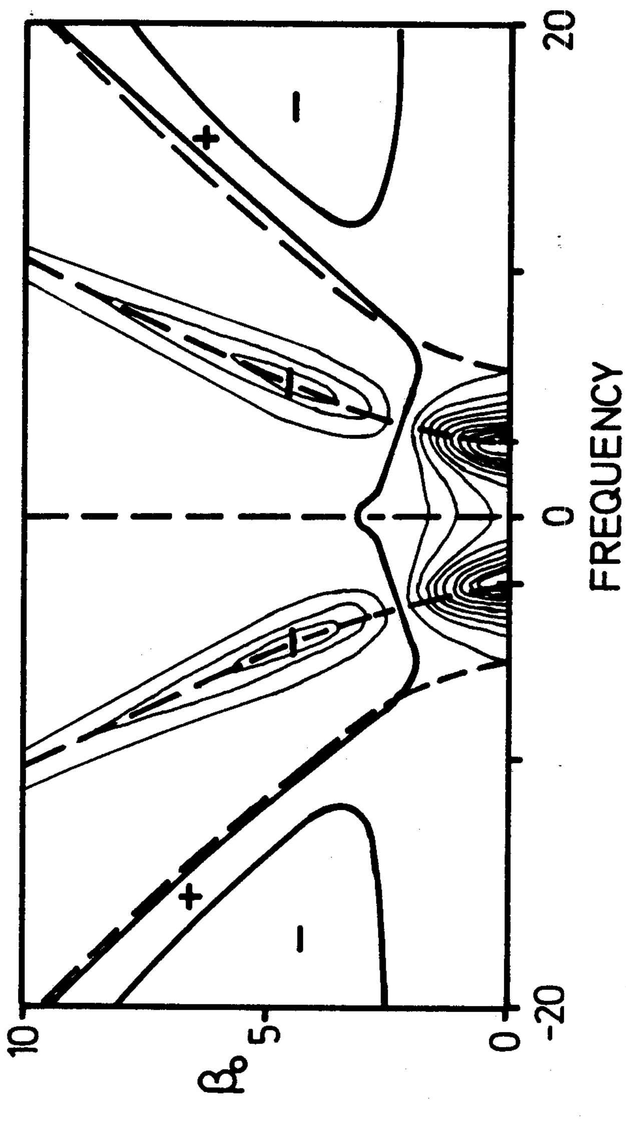

Fig 13

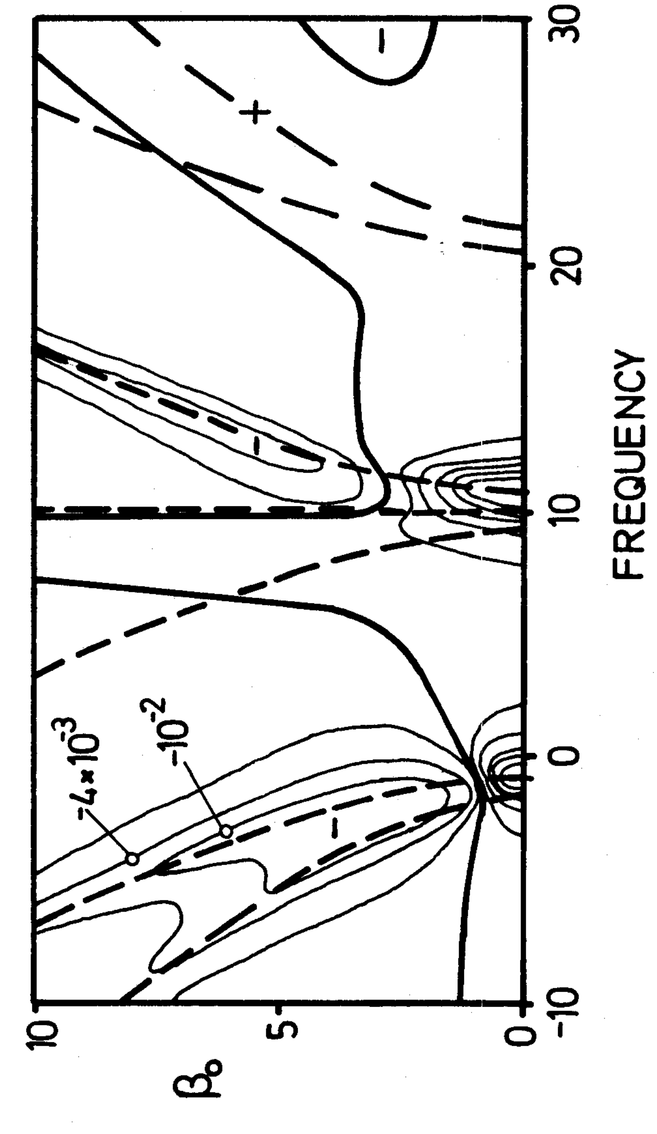

Fig 14